Upper Limb Fossils of Homo naledi from the Lesedi Chamber, Rising Star System, South Africa

Feuerriegel, Elen M ; Voisin, J L ; Churchill, S ; Haeusler, Martin ; Mathews, Sandra ; Schmid, P ; Hawks, J ; Berger, L R

DOI: https://doi.org/10.4207/PA.2019.ART134

Upper Limb Fossils of *Homo naledi* from the Lesedi Chamber, Rising Star System, South Africa

ELEN M. FEUERRIEGEL
Primate Evolutionary Biomechanics Laboratory, Department of Anthropology, Box 353100, University of Washington, Seattle, WA 98195-3100, USA; and, Evolutionary Studies Institute and Centre for Excellence in Palaeosciences, University of the Witwatersrand, Private Bag 3, Wits 2050, SOUTH AFRICA; efeuer@uw.edu

JEAN-LUC VOISIN
Aix Marseille Université, CNRS, EFS, ADES, Marseille, FRANCE; jeanlucvoisin2004@yahoo.fr

STEVEN E. CHURCHILL
Department of Evolutionary Anthropology, Box 90383, Duke University, Durham, NC 27708, USA; and, Evolutionary Studies Institute and Centre for Excellence in Palaeosciences, University of the Witwatersrand, Private Bag 3, Wits 2050, SOUTH AFRICA; churchy@duke.edu

MARTIN HAEUSLER
Institute of Evolutionary Medicine, University of Zürich, Winterhurerstr. 190, CH-8057 Zürich, SWITZERLAND; Martin.Haeusler@iem.uzh.ch

SANDRA MATHEWS
Institute of Evolutionary Medicine, University of Zürich, Winterhurerstr. 190, CH-8057 Zürich; and Paul Scherrer Institut, CH-5232 Villigen, SWITZERLAND; sandra.mathews@psi.ch

PETER SCHMID
Anthropological Institute and Museum, University of Zürich, Winterthurerstr. 190, CH-8057, SWITZERLAND; and, Evolutionary Studies Institute and Centre for Excellence in Palaeosciences, University of the Witwatersrand, Private Bag 3, Wits 2050, SOUTH AFRICA; smidi@aim.uzh.ch

JOHN HAWKS
Department of Anthropology, University of Wisconsin-Madison, Madison, WI 53593, USA; and, Evolutionary Studies Institute and Centre for Excellence in Palaeosciences, University of the Witwatersrand, Private Bag 3, Wits 2050, SOUTH AFRICA; jhawks@wisc.edu

LEE R. BERGER
Evolutionary Studies Institute and Centre for Excellence in Palaeosciences, University of the Witwatersrand, Private Bag 3, Wits 2050, SOUTH AFRICA; Lee.Berger@wits.ac.za

submitted: 3 December 2018; accepted 5 March 2019

ABSTRACT

Homo naledi skeletal material described from the Dinaledi Chamber, Rising Star System, in the Cradle of Humankind, South Africa, includes upper limb material with remarkably ape-like morphology occurring in the context of a distinctly modern human-like lower limb, foot, and hand. Here we describe upper limb specimens from a new fossil hominin site within the Rising Star System, the Lesedi Chamber (Site U.W. 102), including an intact clavicle and a well-preserved proximal humerus and proximal ulna. Craniodental remains, in association with the postcranial elements described here, have been attributed to *H. naledi.* The upper limb material from the Lesedi Chamber is gracile and resembles the upper limb material from the Dinaledi Chamber in overall morphology. The primitive humeral morphology of the Dinaledi material is replicated within the Lesedi material. The fossils from the Lesedi Chamber material also preserve additional humeral morphology not represented in the Dinaledi Chamber, providing new information on humeral form in this species. Three-dimensional geometric morphometric analysis of the Lesedi proximal humerus demonstrates affinities with the humeri of *Pan* and *Australopithecus.* The complete clavicle from Lesedi is similarly primitive, supporting previous interpretations of the *H. naledi* shoulder as being more superiorly positioned than modern humans, and closer to the hypothesized australopith condition. The ulna is gracile, with a mediolaterally narrow olecranon process and anterior-facing trochlear notch similar to the derived state suggested for other fossil hominins. These new findings support the interpretation of overhead reaching and climbing behaviors having continued relevance in the locomotor repertoire of *Homo naledi* and provide a clearer picture of the upper limb morphology of this species.

  ISSN 1545-0031
doi:10.4207/PA.2019.ART134

INTRODUCTION

The modern human upper limb is unique among primates in functioning almost exclusively as an organ of manipulation rather than prehension related to locomotion. The commitment of the human forelimb to manipulation is reflected in its musculoskeletal morphology; however, the point in our evolutionary history where the human upper limb went from a structure used predominantly in locomotion to one used predominantly in manipulation is unclear. Primitive upper limb features in certain ancestral species are interpreted by some authors to indicate a continued reliance on the upper limb for climbing and suspension, and interpreted by others as adaptively inconsequential primitive retentions in habitual terrestrial bipeds. New fossil material and new analyses are providing greater resolution on the meaning of evolutionary changes in upper limb morphology in the hominin lineage.

Previous work on early members of the genus *Homo* (fossils dated to approximately 2–1 Ma, including OH 7, OH 48, OH 62, KNM-ER 3735, KNM-WT 15000, and the Dmanisi hominins) has indicated the beginning of a temporal trend within the genus *Homo* for decreasing involvement of the upper limb in locomotive behaviors and an increasing commitment to manipulation and prehensile movements of the hand (e.g., Jashashvili 2005; Leakey et al. 1989; Lordkipanidze et al. 2007; Napier 1965; Oxnard 1969; Voisin 2008). This Early Pleistocene material is variable in its expression of primitive and derived upper limb morphology, with some traits suggestive of continued use of the upper limb in locomotion and others reflecting an emphasis on manipulation. By the Middle Pleistocene, the complete decoupling of the arm from the constraints of locomotion in *Homo* is characterized by, among other things, a lowering of scapular position on the thorax from the high position seen in australopiths, a lateral orientation to the scapular glenoid fossa, relatively long claviculae, a proximally-oriented ulnar olecranon process, and changes in manual proportions (Drapeau 2008; Larson 2007, 2013).

Precisely when the modern human shoulder and upper limb configuration first arose remains an open question and there are competing models for the trajectory of upper limb (shoulder, elbow, and hand) configuration in the genus *Homo* (e.g., see Larson 2007; Roach et al. 2013; Roach and Richmond 2015). Nevertheless, it is generally accepted that by at least 800 ka a basically modern human-like upper limb arrangement was in place with the emergence of *Homo antecessor* (Carretero et al. 1997; Carretero et al. 1999; Lorenzo et al. 1999; Marzke 1997; Susman 1998). While they exhibit some variation away from modern humans in terms of morphological particulars (variations that may reflect performance differences in certain manipulatory behaviors but not capability differences; Niewoehner 2000, 2001), *Homo heidelbergensis* and *Homo neanderthalensis* also display a human-like shoulder and upper limb configuration, and total freedom of the upper limb from the constraints of locomotion—a scapula positioned low on the thorax with a laterally-oriented glenoid fossa, a relatively long clavicle, a proximally-oriented ulnar olecranon process, and a basically human-like hand (Arsuaga et al. 1997; Carretero et al. 1997; Churchill and Trinkaus 1990; Niewoehner et al. 1997; Trinkaus 1977; Trinkaus 1983; Trinkaus and Villemeur 1991; Vandermeersch and Trinkaus 1995). Even *Homo floresiensis* (initially recovered only from Late Pleistocene contexts (Sutikna et al., 2016), though recent discoveries from Mata Menge might represent a Middle Pleistocene occurrence of this species (van den Bergh et al. 2016)), appears to have been a committed biped with limited evidence for climbing as a major component of its locomotor repertoire, despite maintaining a primitive shoulder configuration (for more details, see Larson 2007).

Contravening this upper limb pattern for Middle Pleistocene *Homo* is *Homo naledi.* Previous work on the upper limb material attributed to *H. naledi* from the Dinaledi Chamber in the Rising Star cave system (Gauteng Province, South Africa) suggested that *H. naledi* exhibited a suite of markedly primitive morphologies (Feuerriegel et al. 2017), and these traits were indicative of continued involvement of the upper limb in locomotion (Kivell et al. 2015). Dated to 335–236 ka (Dirks et al. 2017), *H. naledi* appears to represent an exception to an otherwise robust pattern of non-involvement of the upper limb in locomotion among Middle Pleistocene members of the genus *Homo.* Functional interpretations of the Dinaledi upper limb fossils have been, however, hindered by the fragmentary nature of the material. The discovery of more complete upper limb elements from a new chamber in the Rising Star cave system, the Lesedi Chamber, provides new information about the forelimb anatomy of this recently-discovered primitive member of the genus *Homo*. This chamber is within the same cave system as, and in close geographical proximity to, the *H. naledi* material described by Berger et al. (2015) from the Dinaledi Chamber. Craniodental comparisons to the Dinaledi Chamber materials (Hawks et al. 2017) referred this new material from Lesedi to *H. naledi.*

The Lesedi Chamber is designated as Site U.W. 102 (hereafter Site 102), and its assemblage comprises 131 hominin specimens from at least 3 individuals across both adult and immature developmental stages. This includes 16 identifiable fragments of claviculae, scapulae, humeri, radii, and ulnae, of which 13 preserve diagnostic anatomy (see Figures 1–5 below; see Tables 1–3 below). The most complete of these elements are attributable to the large adult individual, designated LES 1, from collection area 102a (Hawks et al. 2017). Here we present detailed comparisons of the Lesedi Chamber upper limb material with upper limb material from the Dinaledi Chamber, and with extant and fossil comparative samples.

ANATOMICAL DESCRIPTIONS OF DIAGNOSTIC FOSSILS

The following descriptions pertain to the diagnostic clavicular, scapular, humeral, radial, and ulnar specimens within the Site 102 assemblage, including their preservation, with reference to comparable specimens from the Site 101/Dinaledi Chamber assemblage described in Feuerriegel et al. (2017) (see Figures 1–5 below; see Tables 1–3 be-

low). Descriptions of remains lacking morphology relevant to functional diagnosis can be found in the Supplementary Information. All measurements are in millimetres (mm).

CLAVICULAE

U.W. 102a-021 (Figure 1, Table 1)
U.W. 102a-021 is a largely complete right clavicle missing only the surface of the sternal epiphysis. Trabecular bone is exposed over the entire sternal articular area, including a small section of the anterior surface. The shaft is broken at the level of the approximate midshaft, however, the two pieces refit cleanly. The acromial end of the clavicle has also undergone some damage, exposing trabecular bone at the lateral-most extremity. Despite the damage to either end, the bone looks largely intact, and length estimates should not be off by more than a few millimetres. On the dorsal surface, the medial part of the crest for the conoid tubercle is broken off in a segment 15.1mm in length. For the following shape descriptions and measurements, the clavicle was oriented with the anteroposterior axis of the acromial end of the clavicle held in a horizontal plane.

The maximum length of the clavicle (M-1: Martin and Saller 1957) is 108mm, and conoid clavicular length (distance between the midpoint of the sternal articular surface and the middle or most projecting point on the conoid tubercle: Churchill 1994) is 86.8mm. Both of these dimensions were measured without making any compensation for missing articular bone, such that the total undamaged dimensions are likely to be 1–2mm greater. Midshaft circumference is 30.0mm and the robusticity index (see Table 1) is 27.8. The sternal end is a narrow oval, with its long axis oriented anterosuperiorly (AS) to posteroinferiorly (PI), at about 108° to the horizontal, in the sagittal plane. The sternal end measures 19.7mm AS-PI by 10.6mm AI-PS (anteroinferiorly to posterosuperiorly). At the midshaft, the diaphysis is 10.2mm superoinferiorly (SI) by 8.4mm anteroposteriorly (AP). The shaft at this position has a gently rounded superior surface and a mildly concave inferior surface, and the anterior face of the shaft is wider SI (8mm) than is the posterior face (ca. 6.5mm), giving the cross-section a D-shape.

The facet of the costo-clavicular or rhomboid ligament presents as a mediolaterally (ML) elongated, raised, and moderately-rugose surface. It is 22.8mm in length measured ML and varies in AP width from 7.8mm at the sternal end to 9.0mm at its most lateral extent. The facet is discrete and does not appear to grade into the sternal epiphysis. Torsion is evident in the shaft, such that the superior surface of the acromial end faces primarily in a dorsal direction when the costo-clavicular ligament facet is held with the facet facing directly inferiorly, as it does in modern humans. This suggests posterior expansion of the rhomboid facet unlike that of modern humans. When viewed cranially in physiological position (that is, with the acromial end of the clavicle held in a horizontal plane), there is a moderate sigmoid curvature to the clavicle. In dorsal view, the acromial extremity of the clavicle inflects inferiorly.

As with clavicular specimens from the Dinaledi Chamber (Site 101), the overall appearance of the clavicle is smooth, with only a few weakly developed entheses. The deltoid crest is present as a mildly rugose line on the anterior surface of the lateral curvature. The conoid tubercle appears well-developed and forms a posteriorly projecting flange, producing a pronounced border to a moderately deep subclavian sulcus, as in three of the four already known claviculae from the Dinaledi Chamber (U.W. 101-258, U.W. 101-1229, and U.W. 101-1347; the fourth is not complete enough to evaluate this trait (Feuerriegel et al. 2017)). Unlike the specimens from the Dinaledi Chamber (e.g., U.W. 101-258), however, the conoid tubercle is not centrally positioned on the shaft, but rather occurs on the posterior margin. On U.W. 102a-021, the subclavian sulcus is present as a groove on the inferior aspect of the shaft. Damage to the medial part of the conoid flange prevents an assessment of the nature of the transition from the superior to the posterior surfaces, although it appears likely that the two surfaces were distinctly demarcated from one another by a crest. The clavicular insertion for *m. trapezius* on the posterosuperior surface is indistinct. On the anteroinferior surface, a mildly rugose ridge of bone extends from the conoid tubercle laterally to the acromial end. This ridge is relatively wide (varying between 3.5–6.0mm AP).

When the acromial end is held horizontally, the center of the sternal end is about 20mm lower than the acromial end, indicating that there is an overall medioinferior to laterosuperior orientation to the clavicle—an elevated clavicle. The acromial end is a rounded oval, measuring 12.7mm AS-PI by 9.0mm PS-AI. There does not appear to be a distinct facet for the acromion, however damage to the lateral extremity of this specimen may have obscured this feature.

U.W. 102a-239 (see Figure 1)
U.W. 102a-239 is a left clavicle acromial end, 51.5mm in length, and preserving the conoid tubercle (but not its medial crest) and the articular surface for the acromion of the scapula. This specimen is slightly larger and narrower AP than the acromial end of U.W. 102a-021.

As in U.W. 102a-021, the conoid is posteriorly positioned, and produces a posteriorly projecting flange. There is a laterally-running ridge of bone that extends from the conoid tubercle towards the acromion end. The deltoid origin is a moderately rugose line on the anterior margin of the acromial end, while the *m. trapezius* insertion is indistinct. The acromial end has an ovoid shape, and measures 15.6mm AS-PI by 9.5mm PS-AI. The articular surface for the acromio-clavicular joint is visible, and the joint surface looks convex rather than planar.

SCAPULAE

U.W. 102a-010 (Figure 2)
U.W. 102a-010 is a right partial acromion process 53.2mm in total length, preserving the lateral part of the root of the acromion with a small bit of the scapula body (including a very small portion of the ventral surface of the scapula

Figure 1. Clavicular material from the Lesedi Chamber/Site 102a attributed to the LES 1 individual. **a)** *U.W. 102a-021 complete right clavicle;* **b)** *U.W. 102a-239 left acromial clavicular fragment, both in (top to bottom) superior, anterior, inferior, and posterior anatomical views. Far right: medial (top) and lateral (bottom) views with anterior toward the far right of the image.*

TABLE 1. LINEAR DIMENSIONS (mm), INDEX, AND CURVATURE MEASUREMENTS (ratios) OF THE U.W. 102a-021 CLAVICLE.

	U.W. 102a-021
Total length (1)	108
Estimated actual length	110
Supero-inferior (SI) diameter at midshaft (2)	8.2
Antero-posterior (AP) diameter at midshaft (3)	10.2
Diaphyseal index[a]	80.4
Circumference at midshaft (4)	30.0
Robusticity index[b]	27.8
Conoid length	86.8
Nutrient foramen position	56.3
Conoid (SI) diameter	11.2
Conoid (AP) diameter	14.6
Circumference at the conoid tubercle	36
Sternal epiphysis maximum diameter (AP)	19.7
Sternal epiphysis minimum diameter (SI)	10.6
Acromion breadth (AP)	11.5
Acromion height (SI)	8.5
Subclavian sulcus	present
Costo-clavicular facet	present
Clavicle Curvatures[c]	
Acromial (external) curvature	11.6
Sternal (internal) curvature	7.7
Inferior curvature	12.5
Superior curvature	13.4

[a]Diaphyseal index calculated as (2)/(3)*100.
[b]Robusticity index calculated as (4)/(1)*100.
[c]Clavicle curvatures were determined using the Olivier method (Olivier 1951; Voisin 2006a).

body) and the posterolateral part of the acromion process itself. Based on the preserved portion of scapula body, the spine of the scapula appears to have projected out from the scapula body at approximately 90°, though we cannot measure this angle precisely based on the incompleteness of the specimen. The most complete scapular specimen from the Dinaledi Chamber, U.W. 101-1301, has a scapular spine that projects approximately 87° from the long axis of the body, which is comparable to the estimated spine projection for U.W. 102a-010. The insertion line for *m. trapezius* appears rugose but otherwise this specimen is largely non-diagnostic.

U.W. 102a-247

U.W. 102a-247 is a heavily abraded right scapular coracoid process, approximately 24mm in length, measured root to tip. The coracoid tip has some damage in the form of abrasion, as does the superior and medial surface, resulting in some loss of length. The overall size and projection of the coracoid is weak—projection of the process from the root measured inferiorly is ca. 10–12mm. The complete tip would likely add an additional 2–3mm in length, bringing the estimated projection of the coracoid to ca. 15mm.

The specimen preserves the margin of the dorsolateral tubercle. The development of the tubercle is difficult to establish due to poor preservation (much of the tubercle

Figure 2. Scapular material from the Lesedi Chamber/Site 102a attributed to the LES 1 individual. **a)** *U.W. 102a-010 right partial acromion process. Left side of the image, top to bottom: inferior, inferolateral, superior, and medial views. Right side of image: ventral (top) and dorsal (bottom);* **b)** *U.W. 102a-279 left partial glenoid fossa. Left side of the image, top to bottom: inferior, dorsal, superior, and ventral views. Right side of image: lateral (top) and medial (bottom);* **c)** *U.W. 102a-284/256 refitted acromion process and scapular spine. Top to bottom: inferior, dorsal, superior, and ventral views.*

is heavily abraded). What does remain gives the impression of being quite rugose and possibly projecting above the superior surface of the tip in a noticeable manner; the anterior-most margin of the tubercle is pronounced and somewhat bulging.

U.W. 102a-279 (see Figure 2)
U.W. 102a-279 is a fragment of a left scapular glenoid. This specimen preserves only the anteroinferior margin of the glenoid, including a small portion of the anterior surface of the neck of the glenoid. It appears to be from a similarly-sized individual as U.W. 101-1301 from Site 101, however, little else can be said about it.

U.W. 102a-284/256 (see Figure 2)
U.W. 102a-284/256 is a left acromion process preserving a portion of the scapular spine and ventral surface of the scapula/subscapular fossa. This specimen has been refitted from two fragments—U.W. 102a-284 represents the acromion process and U.W. 102a-256 is the scapular spine portion. Both portions have been abraded, but refit well. The lateral surface of the neck of the acromion process has been significantly abraded such that trabecular bone is exposed at the base of the scapular spine. The margins of the acromion process have also been damaged, exposing trabecular bone at its tips.

The insertion for *m. trapezius* and the origin of the posterior portion of *m. deltoideus* appear rugose where they are present on the superior surface of the acromion, but damage to the spine means the morphology of their dorsal-most attachment cannot be determined.

HUMERI

U.W. 102a-002 (Figure 3, Table 2)
U.W. 102a-002 is a right proximal humeral shaft fragment, ca. 85mm in total length, and preserved from the metaphyseal region proximally to somewhere proximal of midshaft (ca. 55–60% of length from the distal end). The head and greater tubercle are missing, as is all but the very base of the lesser tubercle. The distal end of the intertubercular groove is smooth and shallow, and the insertion lines for *mm. pectoralis major*, *latissimus dorsi*, and *teres major* are visible but not especially rugose. The dimensions of the shaft at the distal break (assuming that the head is dorsally oriented, and thus the intertubercular groove is ventral and medial) are 16.2mm AP by 16.4mm ML. Cortical bone thickness at the same point is 5.1mm anteriorly, 4.3mm posteriorly, 4.3mm medially, and 5.3mm laterally.

U.W. 102a-013
U.W. 102a-013 is a fragmentary right humeral head, most probably from the same element as U.W. 102a-002, but has no conjoining surfaces with that specimen. This specimen is comprised of two fragments of articular surface of a humeral head, each with attached articular subchondral bone. These are thought to represent the right humerus because the left humeral head (U.W. 102a-257) is largely intact. The curvatures of the fragments are consistent with the curvatures of the articular surface of U.W. 102a-257, such that U.W. 102a-013 is unlikely to represent a femoral head or other articular surface.

U.W. 102a-257 (see Figure 3, see Table 2)
U.W. 102a-257 is a left proximal humerus, including the humeral head and proximal shaft. This specimen is largely complete from the head to the approximate level of the midshaft (broken at the distal extremity of the deltoid tuberosity). There is erosion to the superior extremity of the articular surface of the head and to the articular margin of the superolateral head, precluding measurement of the head SI diameter. The proximal 40mm or so of the medial and lateral crests of the deltoid tuberosity are present. The anterior surface of the diaphysis exhibits some damage near the distal end of the *m. pectoralis major* crest. The orientation of the bone for measurements was taken as similar to the near-complete Dinaledi Chamber specimen U.W. 101-283. That specimen has a low torsion angle (close to 90°), and we have used this orientation to maximize comparability.

The humeral head has a notably round contour. The transverse breadth of the head (M-9: Martin & Saller 1957) is 33.0mm; the vertical diameter of the head would have been quite similar. Measuring from the inferior articular margin at the midline of the head to the proximal beginning of the insertion of *m. supraspinatus*—as preserved—gives a vertical head diameter (head SI diameter: Churchill 1994) estimate of 33.4mm. The ML arc (M-9b: Knussmann 1988) of the articular surface measures 51mm. The insertions of *mm. supraspinatus* and *infraspinatus* on the proximal surface of the greater tubercle are smooth. Greater tubercle length (measured from the superior margin of the tubercle with the bicipital groove to the most inferior point dorsolaterally) is 28.9mm, with a maximum breadth (greater tubercle projection) of 10.9mm. The greater tubercle does not project superiorly beyond the head. There is some negligible inferoanterior displacement of the superior portion of the greater tubercle via compression, however, not enough to alter the morphology in any appreciable manner.

The bicipital groove appears deep (4.5mm at a point of greatest projection of the tubercles), similar to the most complete humeral specimen from the Dinaledi Chamber, U.W. 101-283. The lesser tubercle is salient, with a breadth of ca. 6.8mm. The attachment area of *m. subscapularis* is largely smooth. The crest extending distally from the lesser tubercle as the insertion for *mm. latissimus dorsi* and *teres major* is slightly better developed in this specimen than the right side (U.W. 102a-002), as is the crest of the greater tubercle where *m. pectoralis major* inserts. The maximum neck diameter is 17.7mm, minimum diameter is 15.8mm. Humeral torsion in this specimen has been estimated at 123.1°; see below for details on how this estimate was acquired and a discussion of the result.

Moving distally, the remaining portion of the deltoid tuberosity presents as a distinct depression with clear margins. These margins are expressed as moderately rugose ridges. At the distal point of breakage, the dimensions of

Figure 3. Humeral material from the Lesedi Chamber/Site 102a attributed to the LES 1 individual. Left to right: posterior, lateral, anterior, and medial views. Far right: superior and inferior views with the anterior aspect towards the top of the image. **a)** *U.W. 102a-257 left proximal humerus including head and tubercles;* **b)** *U.W. 102a-002 right proximal humeral shaft.*

the shaft are 17.3mm AP by 15.0mm ML. Cortical bone thickness at the same point is 6.9mm anteriorly, 4.1mm posteriorly, ca. 3.0mm medially, and 4.9mm laterally. Shaft circumference at this location is 54mm.

ULNAE

U.W. 102a-015/020 (Figure 4, Table 3)
U.W. 102-015 is a right proximal ulna, 148mm in total length, preserving much of the trochlear notch and olecranon process proximally to approximately the midshaft

TABLE 2. HUMERAL DIMENSIONS (mm) IN *HOMO NALEDI* (Site 101 and Site 102) AND COMPARATIVE SAMPLES.*

	U.W. 101-283	U.W. 101-466	U.W. 101-744	U.W. 101-1240	U.W. 102a-257	MH1	MH2	A.L. 288-1	KNM-WT 15000	*H. sapiens* (female, n=52)[f]	*H. sapiens* (male, n=52)[f]	*Gorilla* (n=20)	*Pan* (n=23)
Humeral maximum length	256.0	-	-	-	-	248.0	269.0	236.8[d]	319.0	294.2 (12.9)	323.5 (16.8)	420.4 (41.2)	283.5 (14.7)
Humeral head vertical diameter	(30.2)	-	-	-	(33.4)	34.5	32.3	26.8[d]	29.2	37.9 (2.1)	43.3 (2.7)	57.17 (7.8)	39.5 (2.49)
Humeral head transverse diameter	(26.4)	-	-	-	33.0	28.4	28.1	31.1[d]	34.1	36.5 (1.7)	40.9 (1.9)	50.5 (8.8)	32.3 (2.1)
Humeral head index[a]	(114.6)	-	-	-	96.9	121.5	115.1	116.0	85.6	103.9 (4.5)	105.7 (4.2)	113.8 (5.3)	122.6 (7.5)
Humeral midshaft circumference	48.4	-	-	-	(51)	55.5	55.0	-	55.0[e]	-	-	97.4 (18.3)	74.8 (5.8)
Humeral minimum circumference	47.5	-	-	-	-	50.0	51.0	57.0	-	59.5 (4.3)	66.4 (4.6)	-	-
Maximum midshaft diameter	16.8	-	-	-	17.7	19.0	15.5	-	-	19.7 (1.4)	22.0 (1.7)	-	-
Minimum midshaft diameter	13.3	-	-	-	(15.5)	13.7	15.9	-	-	15.1 (1.6)	17.4 (1.4)	-	-
Medial pillar breadth	6.9	7.3	-	8.6	-	9.6	7.7	-	11.8	-	-	-	-
Lateral pillar breadth	12.9	13.6	-	11.6	-	14.9	14.1	-	17.3	-	-	-	-
Olecranon fossa breadth	19.2	19.6	22.0	22.7	-	23.6	19.6	-	21.0	-	-	-	-
Pillar index[b]	53.5	53.4	-	74.2	-	64.4	54.6	-	68.2	-	-	-	-
MPB/OFB[c]	36.0	37.1	-	38.0	-	40.7	39.3	-	56.2	-	-	-	-

Values in parentheses are estimates.

*Standard deviation values are presented in parentheses for the extant groups.

[a]Humeral head index calculated as (humeral head vertical diameter/humeral head transverse diameter)*100.

[b]Pillar index calculated as medial pillar breadth/lateral pillar breadth.

[c]MPB/OFB: medial pillar breadth/olecranon fossa breadth.

[d]Data from Johanson et al. (1982).

[e]Data from Richmond et al. (2002).

[f]Collected from the Raymond A. Dart Collection, University of Witwatersrand, South Africa.

Figure 4. Ulnar material from the Lesedi Chamber/Site 102a attributed to the LES 1 individual. U.W. 102a-015/020 right proximal ulna including articular surfaces and olecranon process. Left to right: anterior, medial, posterior, and lateral views. Right side, top: superior aspect of U.W. 102a-015/020, anterior towards the top of the image. Right side, bottom: inferior aspect of the distal break, anterior towards top of image.

distally. There is erosion to the ventral tips and margins of the coronoid and olecranon processes, as well as varying degrees of erosion around the medial (large area of erosion) and lateral (small area) margins of the olecranon process. There is also some erosion to the proximodorsal corner of the olecranon.

The preserved aspects of the trochlear notch are similar to other specimens, in which the notch is anteriorly directed, such as A.L. 438-1 and A.L. 288-1. Erosional loss to the margins may alter the precise orientation, but we can exclude a more proximally directed notch as in *Pongo*. The coronoid height (McHenry et al. 1976; measurement 8) is ca. 27mm. The anteroposterior diameter of the olecranon (McHenry et al. 1976: measurement 9) is ca. 25mm and the proximodistal height of the olecranon, as defined by Drapeau (2005), is ca. 7.6mm. Olecranon length (McHenry et al. 1976: measurement 12) is ca. 15.4mm. The medial and lateral surfaces of the trochlear notch drop away from the guiding ridge fairly steeply. Olecranon breadth (M-6: Martin 1928) is estimated at 18.8mm. The radial notch appears to be relatively large, measuring 14.9mm AP by 9.8mm SI. There is a deep sulcus on the proximal shaft medial of the coronoid process, likely for the origin of *m. flexor digitorum profundus* and the ulnar origin of *m. flexor digitorum superficialis*. Likewise, the distal extension of the *m. anconeus* insertion creates a distinct sulcus on the lateral proximal shaft.

The ulnar tuberosity is slightly displaced medially and is defined by a prominent ridge running along its medial margin (this ridge bounds the distal margin of the sulcus on the proximal medial shaft). The supinator crest is large and rugose. The diameter across the supinator crest is 14.9mm, while the diameter of the shaft at the level of the supinator without the crest is 12.3mm. A distinct ridge ending some 40.5mm distal of the distal margin of the ra-

TABLE 3. DIMENSIONS OF ULNAR SPECIMENS ATTRIBUTED TO *HOMO NALEDI* FROM SITE 101 (Dinaledi) AND SITE 102 (Lesedi).*

	U.W. 101-831	U.W. 101-560	U.W. 101-499	U.W. 102a-015
Coronoid process maximum ML diameter[a]	-	13.9	-	(15.5)
Semilunar notch height[b]	-	16.1	-	(17.8)
Olecranon length[c]	-	13.0	-	(15.4)
Olecranon PD height[d]	-	-	-	(7.6)
Trochlear notch orientation	-	-	-	(14°)
Radial notch SI breadth	-	9.4	-	9.2
Radial notch AP breadth	-	11.2	-	13.3
Midshaft ML diameter	-	-	10.8	10.9
Midshaft AP diameter	-	-	11.2	10.9
Ulna midshaft circumference	-	-	34.8	33.3
Distal minimum circumference[e]	28.0	-	29.0	-
Maximum diameter[f]	9.7	-	9.3	-
Distal AP diameter[g]	14.7	-	12.2	-
Ulna head depth[h]	7.2	-	-	-
Styloid ML breadth[i]	4.0	-	-	-
Styloid projection[j]	2.0	-	-	-

Measurements in parentheses are estimates.
*All measurements are in millimetres (mm) unless specified otherwise.
[a]Coronoid process maximum mediolateral diameter, measured from the proximal margin of the radial notch to the medial margin on the coronoid process.
[b]Semilunar notch height or the minimum distance between the anterior projections of the coronoid and olecranon processes.
[c]Olecranon length as measured from the midpoint of the semilunar notch to the height of the proximal-most point on the olecranon.
[d]Proximodistal height of the olecranon process measured from the anterior tip of the anconeal process to the proximal-most surface of the olecranon.
[e]Distal minimum circumference measured inferior to the pronator quadratus crest.
[f]Maximum diameter measured at the level of maximum development for the pronator quadratus crest.
[g]Anteroposterior diameter of the distal epiphysis including the styloid process.
[h]The depth of the head of the ulna anteroposteriorly and excluding the styloid process and non-articular area.
[i]Breadth of the styloid process measured mediolaterally at the tip.
[j]Projection of the styloid process beyond the articular surface of the ulnar head.

dial notch marks the distal extension of the insertion for *m. supinator*. At the approximate midshaft level, the shaft is D-shaped (with the laterodorsal surface straight and the medioventral surface rounded) measuring 10.3mm ML and 10.4mm DV. Diaphyseal circumference at the same point is 33mm.

RADII

U.W. 102a-025/471 (Figure 5)
U.W. 102a-025 is comprised of two fragments that conjoin to form the distal end of a right radius approximately 79mm in length. Both pieces are darkly stained and possibly burned. With the exception of the distal part of the interosseous crest preserved, this specimen is largely non-diagnostic. U.W. 102a-471 is the distal articular end of the radius that preserves part of the ventral shaft (that refits with U.W. 102a-025) and the ulnar and carpal articular surfaces. The dorsal surface of the very distal part of the shaft (on U.W. 102a-471) is missing.

Diaphyseal dimensions at the proximal point of breakage are 12.0mm ML by 10.6mm AP, with a circumference of 36mm. Distally, the ulnar facet is large (12.8mm AP by 8.5mm maximum proximodistally). The lunate and scaphoid facets blend into one another without visible demarcation between them. The AP diameter across the middle of the scaphoid facet is 10.4mm, while the AP diameter across the middle of the lunate facet is 13.5mm.

Figure 5. Radial material from the Lesedi Chamber/Site 102a attributed to the LES 1 individual. **a)** *U.W. 102a-025 distal radial fragment. Left to right: anterior, medial, posterior, and lateral views. Right: superior (top) and inferior (bottom) views with anterior towards the top of the image;* **b)** *U.W. 102a-471 distal radial fragment, including the ulnar articular facet and a portion of the carpal articular surface. Top row, left to right: anterior, medial, and posterior views. Bottom row: inferior view with anterior towards the top of the image;* **c)** *U.W. 102a-025/471 refitted right partial distal radius in anterior view.*

COMPARATIVE MORPHOLOGY: METHODS

CLAVICLE CURVATURES

Comparative clavicle curvature data for modern humans and non-human primates were drawn from collections at the Natural History Museum (London, England), Musée Royal d'Afrique Central (Tervuren, Belgium), Muséum National d'Histoire Naturelle (Paris, France) and Musée de l'Homme (Paris, France). Clavicle samples for comparison are listed in Tables S2–S6 (Supplementary Information) and all measurements and indices are listed in Table S1. The sample termed "Early *Homo*" includes all clavicular remains older than *Homo neanderthalensis*, including the claviculae of KNM-WT 15000 (attributed variously in the literature to *Homo erectus* or *Homo ergaster*), OH 48 (attributed to *Homo habilis*), A63 (*Homo heidelbergensis)*, and ATD 6-50 (*Homo antecessor*), in order to generate a sample of fossil *Homo* claviculae of sufficient size for statistical comparisons (see Table S1 in the Supplementary Information). Notably, all the claviculae in the Early *Homo* sample have

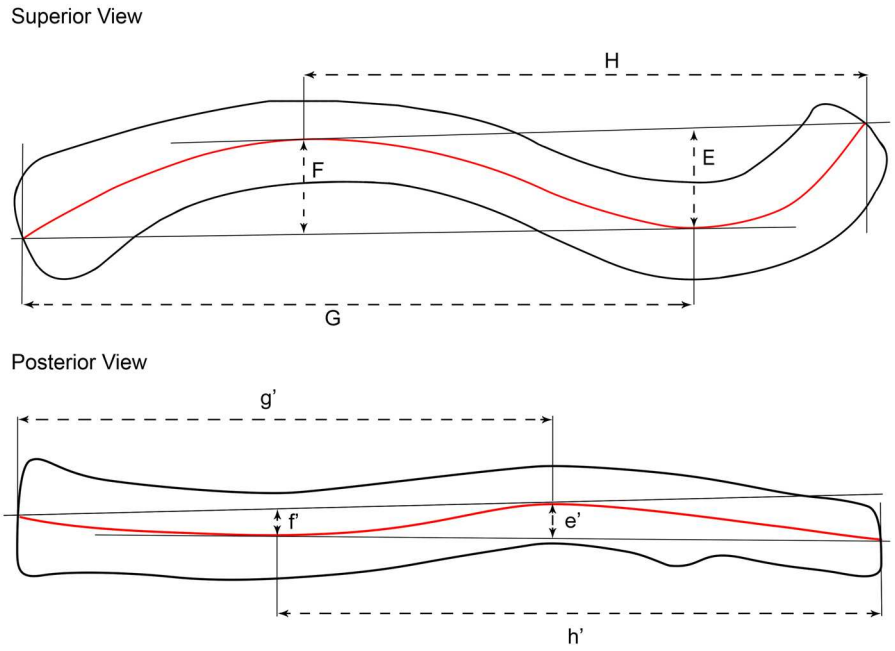

Figure 6. Clavicular chords used for the determination of curvature on a right clavicle from Homo sapiens. Refer to Methods in the main text for an explanation of the clavicle chords.

similar values for metrics taken for this study, reinforcing their inclusion in a single sample group (Voisin and Chevalier in press). The "early modern human" sample includes claviculae of European Upper Paleolithic associated modern humans, as well as those of Qafzeh 9 and Omo I KHS (see Table S2).

The U.W. 102a-021 complete clavicle was used to collect curvature data. Clavicle curvature was measured using the method outlined by Olivier (1951) and Voisin (2000, 2008). A series of chords were defined for the clavicle in both superior and posterior views, and curvature is expressed as a ratio between the height (subtense) of the curvature and the length of the chord. Most hominoid claviculae present four basic curvatures, two in superior view (internal and external) and two in posterior view (superior and inferior; Figure 6). In superior view, chord *H* is the distance between the midpoint of the acromial articulation and the point of greatest internal curvature; chord *G* is the distance between the axis of the sternal articulation and the point of greatest external curvature; subtenses *E* and *F* are the heights of the external and internal curvatures at the point of maximal curvature. In posterior view, the same procedure was undertaken—a central line was traced following the contours of the curvatures through the midpoint of the clavicle. Chord *h'* of the inferior curvature is therefore the distance between the lowest point of the inferior curvature and the vertical axis of the acromial articulation; chord *g'* is the distance between the vertical axis of the sternal articulation and the highest point of the inferior curvature; subtenses *e'* and *f'* are heights of the inferior and superior curvatures at the point of greatest curvature.

Superior curvatures were calculated as:

External curvature = (E/H)100
Internal curvature = (F/G)100

Posterior curvatures were calculated as:

Inferior curvature = (e'/h')100
Superior curvature = (f'/g')100

Box plot graphs and Kruskall-Wallis tests were obtained with PAST 2.17c statistical software. In addition to measures of curvature, clavicular size and shape were quantified using a variety of standard measurements and indices, as detailed in Table 1.

HUMERAL TORSION

Humeral torsion was estimated for U.W. 102a-257 using the regression formulae developed by Larson (1996). Larson found that the single best predictor of torsion in modern human humeri was head size, and as such torsion may be predicted by the equation:

Pred. torsion =7 7.01+1.30(head size)

where head size was formulated as the square root of the product of the vertical humeral head diameter (VHD) and transverse humeral head diameter (THD):

Head size = √((VHD ×THD))

TABLE 4. COMPARATIVE PROXIMAL HUMERAL SAMPLE USED IN THE 3D GEOMETRIC MORPHOMETRIC ANALYSIS AND KNOWN LOCOMOTOR REPERTOIRE FOR EXTANT SPECIES.

Species	*Locomotor Repertoire*	*N*	*Source*
Gorilla gorilla	Terrestrial knuckle-walking	17	AMNH, ANU
Pan troglodytes	Terrestrial knuckle-walking, arboreal climbing and arm-swinging	20	AMNH, ANU
Pongo pygmaeus	Arboreal quadrumanous, arm-swinging	8	AMNH, ANU
Macaca sp.	Terrestrial pronograde quadrupedalism	10	UW
Hylobates sp.	Brachiation	7	UW
Homo sapiens	Bipedalism	15	AMNH, ANU
Australopithecus afarensis (A.L.288-1aml recon.)	Bipedalism. Arboreal climbing, arm-swinging?	1	eLucy.org
Australopithecus sediba (MH2, U.W. 88-57)	Bipedalism. Arboreal climbing, arm-swinging?	1	Wits
Australopithecus sp. (Omo 119-73-2781 1st gen. cast)	Bipedalism. Arboreal climbing, arm-swinging?	1	UW
Homo naledi (U.W. 102a-257)	Bipedalism. Arboreal climbing?	1	Wits
Homo neanderthalensis (Regourdou 1)	Bipedalism	1	NESPOS
	Total	**82**	

AMNH=American Museum of Natural History/Eric Delson; ANU=Australian National University; UW=University of Washington; Wits=University of Witwatersrand.
Gorilla, *Pan*, and *Pongo* humeri in the Delson collection at AMNH originated from wild-shot animals.

As U.W. 102a-257 also preserves the tubercles and the morphology of *H. naledi* humeri more closely resembles australopiths than modern humans, torsion was predicted using the equation used for Sts 7 in the same paper:

Pred. torsion = 44.07+1.38(head size)+0.44(SSIF angle) - 1.52(Subscap.facet width) - 0.19 (Infra.facet angle)

where SSIF angle is the angle formed between a line projected in the plane of the infraspinous facet, and a line projected in the plane of the supraspinous facet. Subscapularis facet width is measured directly on the lesser tubercle of the humerus using calipers. The infraspinous facet angle is the angle formed between a line projected in the long axis of the humeral shaft and a line projected in the plane of the infraspinous facet. The angular measurements were taken on photographs of the specimen. Refer to Larson (1995) for further details about these measures. Comparative data on extant hominoids and extinct hominins were taken from the literature as detailed in Table 11 (below).

PROXIMAL HUMERAL 3D GEOMETRIC MORPHOMETRICS

Three-dimensional geometric morphometric analysis is a useful way of describing the functional anatomical differences between primate taxa, including hominoids and modern humans (Arias-Martorell et al. 2012; 2015a; 2015b; Bookstein 1991). To better place the *H. naledi* shoulder in its appropriate functional context, we collected landmark data on 3D surface scans of a variety of mixed-sex fossil and extant primate proximal humeri, all right-sided (Table 4). Humeral scans from *Gorilla*, *Pan*, *Pongo*, and modern *Homo sapiens* were drawn primarily from Eric Delson's collection at the American Museum of Natural History (AMNH, New York), and supplemented by additional specimens drawn from the collections of the Australian National University, Australia. Humeral specimens attributed to *Macaca* and *Hylobates* were drawn from the primate skeletal collection in the Department of Anthropology at the University of Washington, Seattle, and scanned with a Artec Space Spider® blue-light 3D scanner, and processed using Artec Studio 12 software (Artec 2016). U.W. 102a-257 (left humerus, *Homo naledi*) and U.W. 88-57 (right humerus, *A. sediba*) were scanned using a NextEngine desktop 3D scanner (NextEngine, Santa Monica, CA), and processed using the ScanStudio HD software package (NextEngine 2006). A scan of the A.L. 288-1r left proximal humerus was obtained by M.H. A scan of the reconstructed A.L. 288-1aml right humerus was obtained via the eLucy website by request (https://elucy.org/; Department of Anthropology, University of Texas, Austin) (see also Kappelman et al. 2016). The australopith material was supplemented by a 3D scan of a first-generation, research-quality cast of Omo 119-73-2718, a right humerus attributed to *Australopithecus* sp. (Larson 2007). A

TABLE 5. LANDMARKS USED FOR THE PROXIMAL HUMERAL 3D GEOMETRIC MORPHOMETRIC ANALYSIS (after Arias-Martorell et al. 2012).

Landmark	*Type*[a]	*Description*
Lesser Tubercle		
L1	II	Distal end of the *subscapularis* insertion facet
L2	II	Proximal end of the *subscapularis* insertion facet
L3	II	Lateral point of the *subscapularis* insertion facet
L4	II	Medial point of the *subscapularis* insertion facet
Greater Tubercle		
L5	II	Anterior end of the *supraspinatus* insertion facet
L6	II	Posterior end of the *supraspinatus* insertion facet
L7	II	Lateral point of the *supraspinatus* insertion facet
L8	II	Medial point of the *supraspinatus* insertion facet
L9	II	Distal end of the *infraspinatus* insertion facet
L10	II	Proximal end of the *infraspinatus* insertion facet
L11	II	Lateral point of the *infraspinatus* insertion facet
L12	II	Medial point of the *infraspinatus* insertion facet
L13	II	Distal end of the *teres minor* insertion facet
L14	II	Proximal end of the *teres minor* insertion facet
L15	II	Lateral point of the *teres minor* insertion facet
L16	II	Medial point of the *teres minor* insertion facet
Articular Surface		
L17	II	Intersection point between the articular perimeter and the major prominence of the greater tubercle in posterior/anterior view
L18	II	Maximum point of curvature of the articular perimeter in the mediolateral and anteroposterior plane
L19	II	Most medial point of the articular perimeter
L20	II	Intersection point in the articular perimeter between the lesser tubercle and the articular surface in superior view
L21	II	Intersection in the articular perimeter between the greater tubercle and the articular surface in superior view
SL1	SL	Mid-point between L17 and L18 on the articular surface
SL2	SL	Mid-point between L18 and L19 on the articular surface
SL3	SL	Mid-point between L20 and L18 on the articular surface
SL4	SL	Mid-point between L21 and L18 on the articular surface

[a]Landmark type (I, II, III) assigned according to Bookstein's (1991) classification; SL=Semilandmark.

3D scan of the Regourdou 1 right humerus attributed to *H. neanderthalensis* was obtained from the NESPOS Society digital repository (https://www.nespos.org/display/openspace/Home). All scans were either obtained primarily in, or converted to, file formats suitable for use in Landmark Editor 3.0 (Wiley 2006).

A total of 21 landmarks and 4 semilandmarks were applied to the proximal articular surface and tubercles of the humeri following the procedure outlined by Arias-Martorell et al. (2015a; Table 5), capturing the shape of the articular surface and the tubercles. This procedure was adopted to ensure comparability of the present study with the existing literature and for its suitability for fossil material; only external points of the muscle insertion facets were recorded, avoiding potential erosional effects as a result of taphonomic processes, and the landmarks on the humeral head captured the intact perimeters of the articular surface, preserving homology. The landmarks were located and placed manually using Landmark Editor (Wiley 2006). Landmarks 17 to 21 (the landmarks describing the articular surface) were recorded as three-point curves, automatically generating the semilandmarks and placing them equidistantly between the landmarks on the curve. While most specimens were sufficiently intact to allow for automatic placement of the semilandmarks, U.W. 102a-257 is missing the proximal-most portion of the articular surface. In

TABLE 6. LINEAR MEASUREMENTS USED IN THE ULNAR PRINCIPAL COMPONENTS ANALYSIS.

	Measurement Number in McHenry et al. (1976)
Trochlear AP diameter (TAP)	7
Coronoid height (CHT)	8
Olecranon AP diameter (OAP)	9
Trochlear length (TL)	10
Tuberosity position (TP)	11
Olecranon length (OL)	12
Proximal AP diameter (PAP)	13
Proximal transverse diameter (PTV)	14

this instance, SL1 was marked as a missing data point. The reconstructed A.L. 288-1aml right humerus was chosen for inclusion in this study over the largely-complete A.L. 288-1r left humerus due to completeness of tubercle morphology and, consequently, most of the landmarks used in the analysis. While the humeral head of A.L. 288-1r is more complete than A.L. 288-1aml, the muscle attachment sites for *mm. supraspinatus, infraspinatus, subscapularis,* and *teres minor* were more easily discerned or more complete on the reconstructed humerus. While the contour of the articular surface is intact at the locations of the landmarks and semilandmarks in A.L. 288-1aml, Landmark 19 (most medial point of the articular perimeter) is missing. Nevertheless, the remaining section of the medial perimeter is within ~3mm of the anticipated medial-most point of the articular perimeter based on visual comparison with the more intact articular surface of A.L. 288-1r. While not ideal, the landmark placement on the existing sections of the A.L. 288-1aml articular surface gave a fair approximation of humeral head shape. After all landmarks had been placed and corresponded to the template or reference model (*H. sapiens*), the landmark coordinates (x, y, z) for each specimen were exported for analysis in MorphoJ (Klingenberg 2011).

The raw coordinate data for all comparative samples were transformed using a full Procrustes superimposition to remove the effects of scale, translation, reflection, and rotation, leaving only shape variation. MorphoJ automatically uses a full Procrustes fit to superimpose landmark coordinates, including reflection of corresponding landmark configurations, rather than a partial Procrustes fit (Klingenberg 2011), allowing for the inclusion of both left- and right-side specimens in the analysis. To explore shape variation among primate taxa without imposing *a priori* classification based on inferred functional similarities or phylogeny, a principal components analysis (PCA; computed on a covariance matrix in MorphoJ) was used to ordinate the resultant Procrustes coordinates. PCA scatter plots were generated to visualize changes in skeletal shape related to locomotor behavior by plotting the most informative principal components against one another.

ULNA MULTIVARIATE ANALYSES

To place the morphology of the LES 1 proximal ulna into a comparative perspective, we conducted a PCA with eight linear variables (Table 6) taken on mixed sex samples of fossil and recent modern humans, Neandertals, and other fossil hominins (Table 7). Variables were chosen so as to capture the most salient aspects of proximal ulnar articular and diaphyseal morphology, following Churchill et al. (1996). Linear values were log-transformed and standardized by the geometric mean to produce log-shape values following Darroch and Mosimann (1985). PCAs were conducted using modern human, australopith, and Neandertal data only—PC scores for LES 1 and one additional fossil, KNM-BK 66, were generated from the eigenvectors after the fact. KNM-BK 66 was afforded special treatment because it, like LES 1, is the sole representative of its likely taxonomic group: *H. erectus* (Leakey et al. 1969; Senut 1981; Solan and Day 1992). PCAs were conducted on the correlation matrix using JMP 13 (SAS Institute, Inc., Cary, NC). We tested for morphological similarity between LES 1 and five comparative groups, as defined in Table 7. To do this, we determined the centroid of each comparative group in the three-dimensional space defined by the first four PCs (using the average value of each group on each component as coordinates in three-dimensional space). Euclidean distances were then calculated between the centroid of each comparative group and each fossil, as well as between individuals of each comparative group and their respective centroid. We used a test of a single variate against a group mean (Sokal and Rohlf 1995) to compare LES 1 to the average Euclidean distance within each comparative group (using a one-tailed test with α=0.05). Because *H. naledi* is in many respects morphologically similar to *H. erectus* sensu lato (Dembo et al. 2016; Schroeder et al. 2017), and because the Baringo ulna (KNM-BK 66) represents the only (probable) member of this group, its relationship to LES 1 in morphological shape space is a matter of some interest. We thus also subjected KNM-BK 66 to the same Euclidean distance analysis as applied to LES 1. Because this resulted in pairs of tests (e.g., LES 1 versus australopiths and KNM-BK 66 versus australopiths) that shared variance, we used

TABLE 7. COMPARATIVE SAMPLES USED IN THE ULNAR PRINCIPAL COMPONENTS ANALYSIS (n).

	Comments
Australopiths (5)	
A.L. 288-1	*A. afarensis*. Measurements from cast.
StW 431	*A. africanus.*
MH 1	*A. sediba.*
MH 2	*A. sediba.*
OH 36	*P. boisei?* Measurements from cast.
Neandertals (17)	
Amud 1	
Feldhofer 1	
Kebara 2	
Krapina 179, 181, 182, 183	
La Chapelle 1	
La Ferrassie 1, 2	
Shanidar 1, 4, 5, 6	
Spy 1, 2	
Tabun C1	
Early modern humans (5)	
Klasies River Mouth	Measurements taken on original by O.M. Pearson and F.E. Grine (see Churchill et al. 1996).
Qafzeh 3, 7, 9	
Skhul 4	
Upper Paleolithic modern humans (42)	
Abri Pataud 230, 231	
Arene Candide 2, 3, 4, 5, 10, 12, 15	
Baousso da Torre 2	
Barma Grande 2	
Bruniquel 24	
Cap Blanc 1	
Chancelade 1	
Cro-Magnon 4297, 4300, 4301	
Dolni Vestonice 13, 14, 16	
Gough's Cave 1, 118_01	
Grotte des Enfants 4, 5	
Isturitz 7b	
La Madelaine 1	
La Rochette 1	
Mladec 25c	
Nahal Ein Gev 1	
Neuessing 2	
Oberkassel 1, 2	
Paglicci 25	
Paviland 1	

TABLE 7. COMPARATIVE SAMPLES USED IN THE ULNAR PRINCIPAL COMPONENTS ANALYSIS (n) (continued).

	Comments
Upper Paleolithic modern humans (42)	
Rochereil 1	
Romanelli 1, 1c	
Romito 3, 4	
St Germain la Riviere 4	
Veyrier 1, 9	
Recent modern humans (88)	
Khoisan (7)	Data courtesy of Henry McHenry
Aboriginal Australian (4)	Data courtesy of Henry McHenry
Native American (46)	Data courtesy of Henry McHenry
Inuit/Eskimo (6)	Data courtesy of Henry McHenry
European Americans (25)	

All data collected by SEC on original specimens, unless otherwise noted.

a Bonferroni adjusted alpha of 0.025 (Rice 1989). Centroid analyses were conducted in Microsoft Excel (2013).

TROCHLEAR NOTCH ORIENTATION

Trochlear notch orientation on the incomplete U.W. 102a-015/020 ulna was measured using the method devised by Drapeau (2004) and Haile-Selassie et al. (2010) on a photograph of the lateral aspect of U.W. 102a-015/020 (Figure S1). (To reduce the effects of parallax on the photograph and resultant angular measurements, U.W. 102a-015/020 was positioned in the appropriate aspect on a level horizontal surface and photographed with a remotely-controlled DSLR camera mounted to a spirit-levelled tripod.) This method involves transecting the photograph at the doubled distance from the proximal-most point on the olecranon process to the distal-most edge of the radial facet (see Figure S1). A line was then drawn joining the proximal-most point on the posterior margin of the ulna and the intersection of the transect with the posterior margin of the ulna. The angle between this line and a second line connecting the anterior projections of the coronoid and olecranon processes is the trochlear notch orientation.

While this method tends to slightly overestimate the angle of trochlear orientation if the ulnar shaft was curved, erosional loss, comprising ca. 1–2mm of the coronoid process and slightly less of the anterior tip of the olecranon process, is likely causing minor underestimation of the trochlear notch angle, balancing out the initial overestimation. Consequently, the trochlear notch orientation value presented in this paper can only be considered an estimate.

COMPARATIVE MORPHOLOGY: RESULTS

CLAVICULAR COMPARISONS

Clavicle Curvatures

As with the clavicular remains from the Dinaledi Chamber (Feuerriegel et al. 2017), the curvatures (in superior view) of the Lesedi U.W. 102a-021 clavicle are not especially pronounced; that is, the sigmoid curvature of the clavicular shaft is diminished relative to modern and fossil human samples (as noted above, the *perception* of marked sigmoid curvature of this specimen is created by the posterior projection of the conoid tubercle). In superior view, the acromial (or external) curvature is within the lower ranges of variation of all fossil *Homo* groups, including Neandertals, early modern humans, and early *Homo*. Compared to extant hominoids, the external curvature for U.W. 102a-021 fits well with *Gorilla* curvature values and within the lower extremes of both *Pan troglodytes* and *P. paniscus* (Figure 7). The sternal (or internal) curvature of the *Homo naledi* clavicle is less pronounced than the external curvature at the acromial end, as in all hominoids, but falls within the range of variation of both *Pan* species, in the upper extreme of *Pongo*, and outside *Homo* and *Gorilla* variation (see Figure 7, top). In dorsal view, the inferior (acromial) curvature of U.W. 102a-021 clavicle fits well with the *P. paniscus* variation (see Figure 7, bottom), which corresponds to the most pronounced inferior curvature within hominoids. The superior curvature of the U.W. 102a-021 clavicle in dorsal view is within the highest hominoid values (see Figure 7, bottom) and fits only with the most extreme values of *Pan*

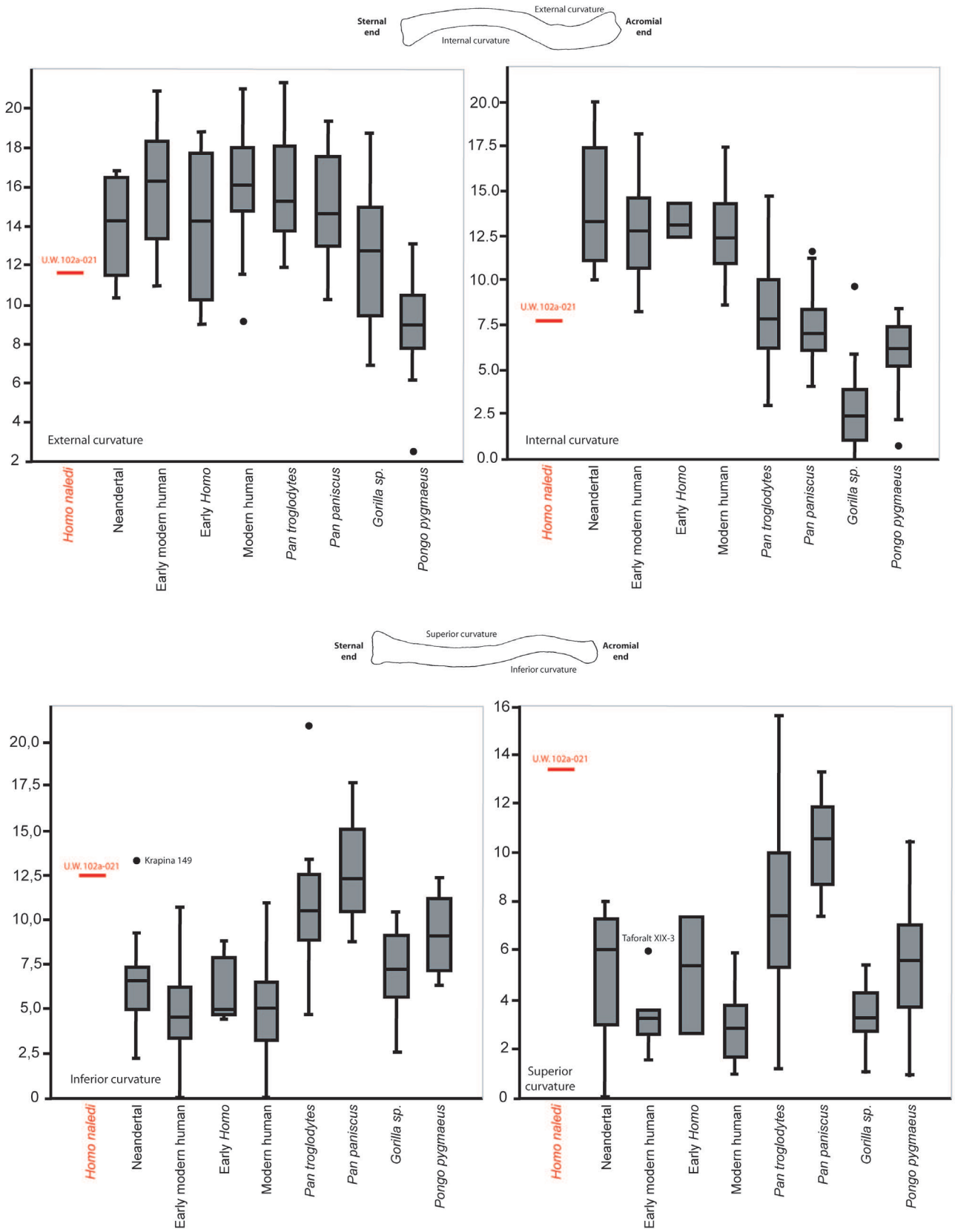

Figure 7. Clavicle curvatures in superior (top frame) and posterior (bottom frame) view within extant hominoids and extinct hominins. Refer to Supplementary Information for details on specimens included in other samples. Within modern humans, only individuals displaying a superior curvature are taken into account (35%). This curvature includes type II and III, the last one exhibited only by Homo *species (Voisin 2001, 2006a).*

TABLE 8. CLAVICLE MORPHOLOGIES AND SHOULDER ARCHITECTURES WITHIN GENUS *HOMO*.*

	Group 1		Group 2
Clavicular Curvatures (posterior view)	Two curvatures		One curvature (or two but slightly pronounced)
	Group 1a	**Group 1b**	
Clavicle Length	Short	Long	Long
Scapula position on the thorax	High Lateral	High Dorsal	Low Dorsal
***Homo* species**	*Homo habilis*, *Homo ergaster/erectus*, ***Homo naledi***	Neandertal *Homo antecessor*	Modern human, Early modern human remains, Anatomically modern human

***Lateral:** The scapula is more laterally placed than in modern humans. **Dorsal:** The scapula is dorsally placed as in modern humans. *Homo naledi* fits best with group 1a (after Voisin 2010).

troglodytes. The presence of pronounced curvatures in dorsal view is associated with high scapular positioning on the thorax (Voisin 2000, 2001, 2006a, 2010) (Table 8), indicating that *H. naledi* likely also had a high scapula position as previously suggested by Feuerriegel and co-authors (2017).

Length and Robusticity

The absolute length of the U.W. 102a-021 clavicle is very short, shorter than that of all great apes, except *P. paniscus* (Figure 8). The U.W. 102a-021 clavicle falls within the lower end of the australopith variation for absolute clavicle length (see Figure 8). Very little can be said about the relative length of the clavicle in *H. naledi* due to the incompleteness of associated thoracic and humeral material with which to make relative length comparisons.

The midshaft circumference of U.W. 102a-021 (see Table 1) is very close in size to the U.W. 101-258 *H. naledi* clavicle (Feuerriegel et al. 2017) (see Table S1). U.W. 102a-021 falls within the lower end of variation for the australopiths in midshaft circumference, though it differs in being slightly larger than that of *A. sediba* (Figure 9) and smaller than KSD-VP-1-1f (Haile-Selassie et al. 2010). KSD-VP-1-1f is the only other australopith clavicle complete enough for an accurate circumference measurement, and it is notably very long and large for an australopith (but see Voisin [2015] for a discussion). Whatever the australopith pattern may be, the circumferences of the two *H. naledi* claviculae are within the lower extreme of variation for all the extant—as well as extinct—hominoids except for *Gorilla* and *Pongo*. This may reflect the small average body size of *H. naledi*. Neandertal and early *Homo* claviculae display a significantly lower clavicular circumferences than early modern humans, but do not differ from modern human claviculae (Table 9). The *H. naledi* clavicular circumference aligns better within the early *Homo* sample for this measurement.

Contrasting with these low circumferential values, the robusticity index in U.W. 102a-021 is comparatively high, indicating that the circumference is not small relative to the total length of the clavicle. Within extant hominoids, *Gorilla* claviculae are significantly more robust than those of other extant hominoids, including modern humans (Table 10). Neandertal, early modern human, *Pan*, *Pongo*, and modern human claviculae are similar in terms of robusticity. The U.W. 102a-021 clavicle is among the most robust claviculae, close to the *Gorilla* median value (Figure 10). U.W. 102a-021 is more robust than Neandertal and early *Homo* claviculae and falls within the range of variation for australopith claviculae.

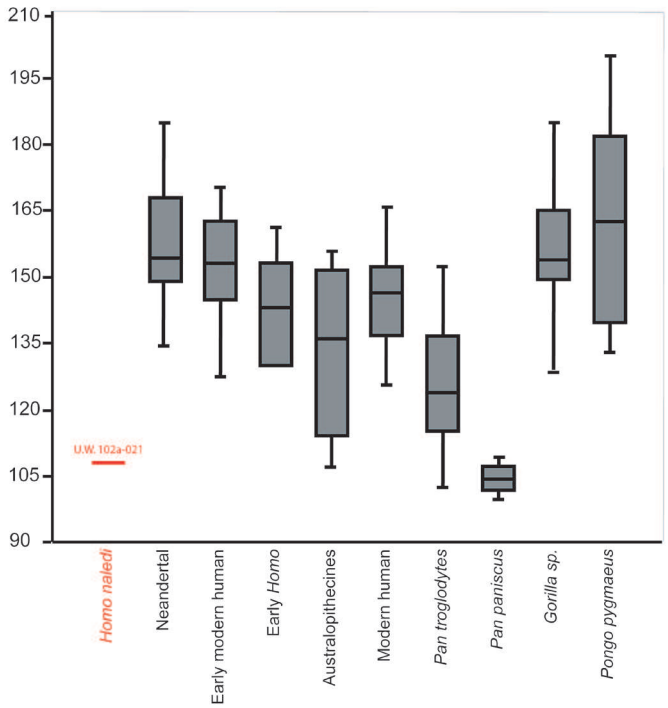

Figure 8. Absolute clavicle length (in mm) in extant hominoids and extinct hominins, including Homo naledi. *Refer to Supplementary Information for details on specimens included in other samples.*

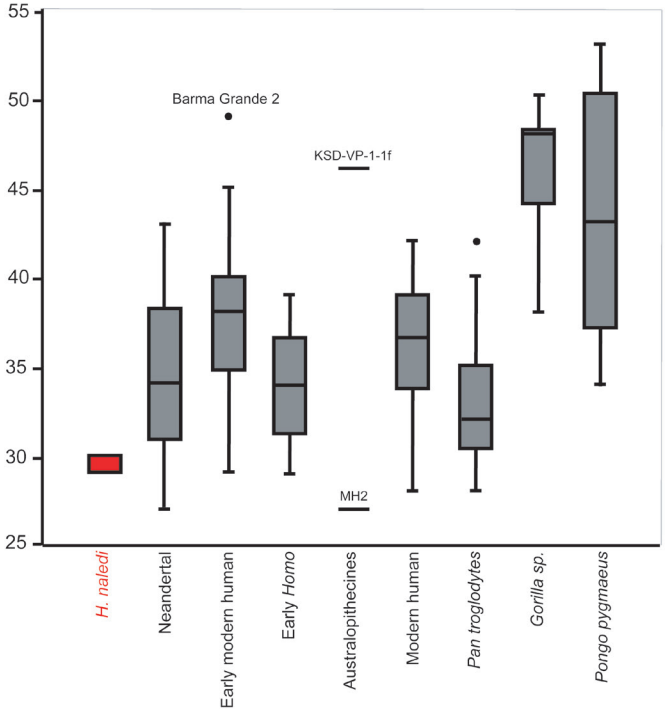

Figure 9. Clavicle circumference (in mm) within extant hominoids and extinct hominins. Homo naledi specimens included are U.W. 101-258 and U.W. 102a-021. Australopithecines included in the analysis are: KSD-VP-1-1 (left side; A. afarensis*) and MH2 (right side;* A. sediba*). The outlier for the early modern human sample is Barma Grande 2 (right side). Refer to Supplementary Information for details on specimens included in other samples.*

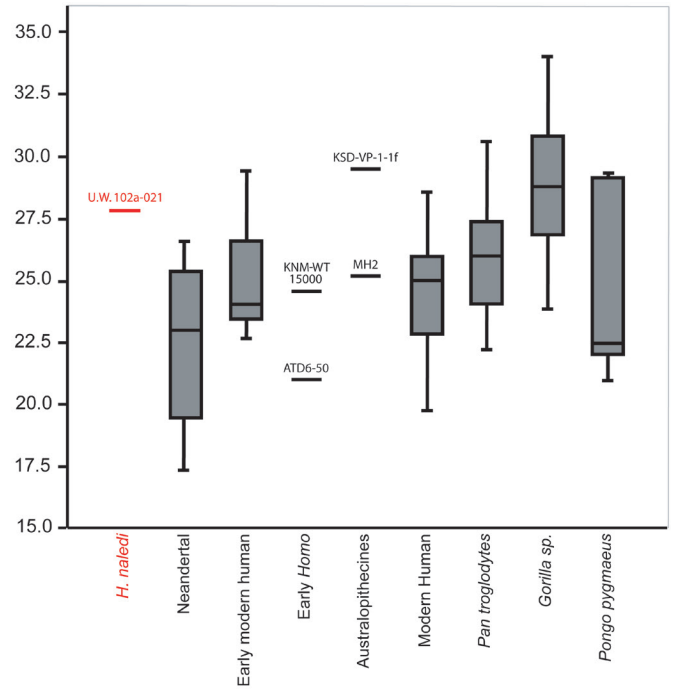

Figure 10. Clavicle robusticity within extant hominoids and extinct hominins. Fossils included in the analysis are: ATD 6-50 (right side; H. antecessor*), KNM-WT 15000 (right side;* H. ergaster*), KSD-VP-1-1 (left side;* A. afarensis*), and MH2 (right side;* A. sediba*). Refer to Supplementary Information for details on specimens included in other samples.*

Costo-Clavicular Facet Morphology

The costo-clavicular ligament/rhomboid facet in U.W. 102a-021 appears large relative to the short absolute length of this clavicle. In modern humans, the length of the costal facet varies between 8mm to 39mm, and the breadth between 3–15mm (Jit and Kaur 1986; Longia et al. 1982). In the U.W. 102a-021 clavicle, the rhomboid facet is 22.8mm in length ML and 7.8–9.0mm in breadth DV, indicating that the dimensions of the facet in U.W. 102a-021 falls in the upper part of modern human variation despite modern human claviculae being much longer in absolute terms.

The rhomboid facet is present more frequently in modern humans (93%) than in great apes (~10–47%), and there is variation in the morphology of this facet between these two groups (Voisin 2000). Modern humans exhibit some variation in rhomboid facet shape but maintain an elliptical contour; the most frequent form in modern human variation is an oval depression (Figure 11a). Apes, on the other hand, exhibit a rhomboid facet that, when present, is slender and grades into the sternal epiphysis (see Figure 11). Within great apes, the rhomboid facet is present most frequently in *Gorilla* (~47%) but still at a much lower in frequency than in modern humans (see Figure 11, bottom). In claviculae that are sufficiently preserved, early modern humans also display a modern human-like rhomboid facet. Neandertals are more variable, with >85% of claviculae exhibiting a rhomboid facet, the morphology of which is modern human-like (see Figure 10, see Table S1). Otherwise, there is no information in the literature about rhomboid facet frequency or morphology within the australopithecines and *Ardipithecus* (see Table S1).

Subclavian Sulcus and Conoid Tubercle Morphology

The subclavian sulcus is present as a groove on the inferior aspect of the shaft of U.W. 102a-021, as on all other *Homo naledi* claviculae sufficiently preserved (e.g., U.W. 101-1347, U.W. 101-258, and U.W. 101-1229) (Feuerriegel et al. 2017). As with the rhomboid facet, the subclavian sulcus is present at a higher frequency within modern human claviculae (80%) than in apes (~23–37%; see Figure 11). The difference between apes and modern humans is not as marked as for the costo-clavicular ligament facet, but is still important (Voisin 2000). Within fossils, almost all Neandertal claviculae display a subclavian sulcus (Figure 12), as do the claviculae of KNM-WT 15000 and Arago 63 (Voisin and Chevalier in press). ATD6-50 and OH 48, on the other hand, do not exhibit a subclavian sulcus (Voisin 2000). Within the six *Australopithecus* claviculae currently known, at least two (StW 431 and KSD-VP-1-1f) display a subclavian sulcus (Melillo 2016; Toussaint et al. 2003); no information about the pres-

TABLE 9. KRUSAL-WALLIS TEST FOR CLAVICLE CIRCUMFERENCE.*

	Neandertal	Early Modern Humans	Early *Homo*	Human	*Pan troglodytes*	*Gorilla*	*Pongo pygmaeus*
Neandertal	0	0,02781	0,513	0,3409	0,08907	$1{,}005.10^{-08}$	0,003459
Early Modern Humans	0,584	0	0,01174	0,2351	0,000147	$1{,}754.10^{-07}$	0,02746
Early *Homo*	1	0,2465	0	0,1038	0,3174	$3{,}708.10^{-06}$	0,004185
Human	1	1	1	0	0,00792	$2{,}039.10^{-08}$	0,007043
P. troglodytes	1	0,003088	1	0,1663	0	$1{,}499.10^{-08}$	0,0003146
Gorilla	$2{,}111.10^{-07}$	$3{,}684.10^{-08}$	$7{,}787.10^{-05}$	$4{,}282.10^{-07}$	$3{,}149.10^{-07}$	0	0,1652
P. pygmaeus	0,07263	0,5766	0,08789	0,1479	0,006607	1	0

H=69,34, p(same): $5.208.10^{-13}$

*Values in shaded cells show significant differences (*p*-value set at < 0.05). Refer to Supplementary Information for details about the samples used.

TABLE 10. KRUSAL-WALLIS TEST FOR CLAVICULAR ROBUSTICITY.*

	Neandertal	Early Modern Humans	Human	*Pan troglodytes*	*Gorilla*	*Pongo pygmaeus*
Neandertal	0	0,05978	0,04567	0,00372	$6{,}771.10^{-06}$	0,177
Early Modern Humans	1	0	0,9128	0,1159	$4{,}559.10^{-05}$	0,9535
Human	1	1	0	0,1172	$1{,}864.10^{-06}$	0,7349
Pan troglodytes	0,1339	1	1	0	0,0004142	0,6559
***Gorilla* sp.**	0,0002438	0,001641	$6{,}711.10^{-05}$	0,01491	0	0,09044
Pongo pygmaeus	1	1	1	1	1	1

H=41,62, p(same): $1.595.10^{-06}$

*Values in shaded cells show significant differences (*p*-value set at <0.05). For detail about the sample, see Supplementary Information.

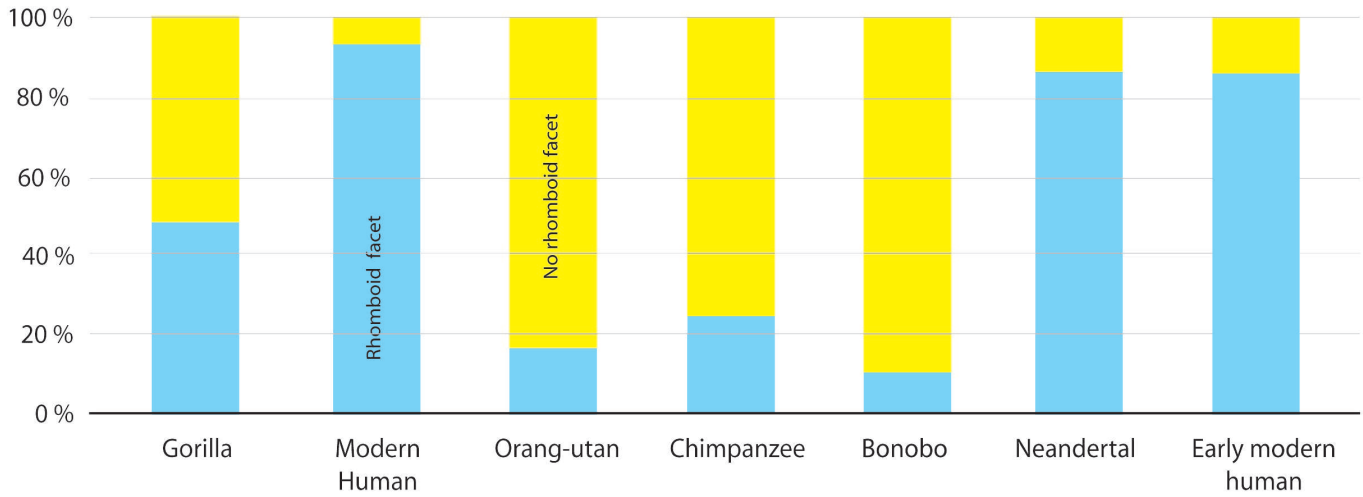

Figure 11. Costo-clavicular ligament, or rhomboid, facet morphology (top) and percentage frequency (bottom) in great apes, modern humans, and U.W. 102a-021. White arrows point to the rhomboid facet in: **a)** H. sapiens*;* **b)** *U.W. 102a-021;* **c)** Pongo pygmaeus*,* **d** *and* **e)** Pan troglodytes*;* **f)** Gorilla *sp. (scale is 2cm [black bar =1cm, white bar=1cm]). Refer to the Supplementary Material for sample sizes in the frequency analysis.*

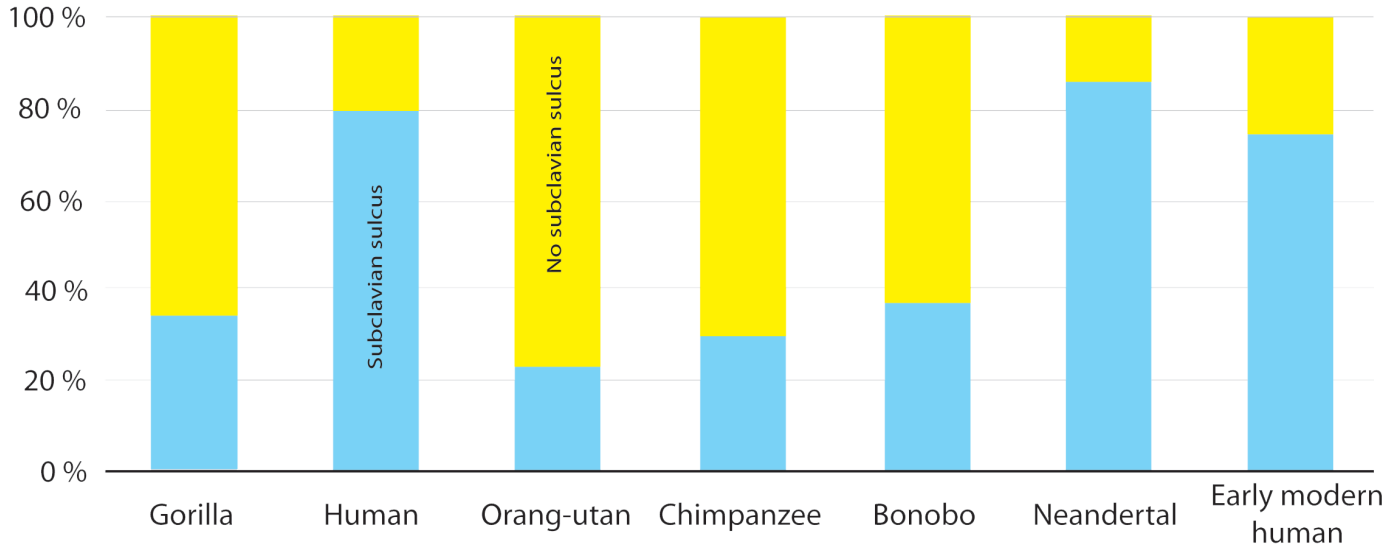

Figure 12. Frequency of subclavian (in %) sulcus within Gorilla *sp. (n=33),* Pongo pygmaeus *(n=23),* Pan troglodytes *(n=24),* Pan paniscus *(n=19), human (n=31), Neandertal (*Homo neanderthalensis*; n=25), and Upper Paleolithic (n=18).*

ence or absence of this characteristic is available for the four additional australopith claviculae. The STD-VP-2/893 clavicle, attributed to *Ardipithecus*, similarly displays a subclavius sulcus (Haile-Selassie et al. 2009). Surprisingly, the frequency of this trait is slightly lower in early modern human remains (74%) than in modern human and Neandertal remains (86%). Olivier (1954) has suggested that increasing clavicular length is correlated with the presence of a subclavian sulcus in modern humans. *Homo naledi* and *A. sediba* claviculae, however, do not corroborate Olivier's (1954) observation due to their very short absolute (and, in the latter case, relative) length. While there is presently no explanation for the observed differences in subclavian groove morphology between modern humans and extant hominoids (the subclavian muscle shows no significant differences in size or attachment between hominoids (Voisin 2000)), the presence of the subclavian sulcus is nonetheless another derived trait present within the *H. naledi* claviculae, and it is possible that this characteristic can be considered derived for the hominin lineage.

The conoid tubercle in U.W. 102a-021 is pronounced in the form of a flange on the posterior margin of the lateral clavicle. In this respect U.W. 102a-021 resembles chimpanzees, differing from modern humans and all *Australopithecus* claviculae except A.L. 438-1 (Drapeau et al. 2005; Partridge et al. 2003). As Larson (2013) observes, there is some diversity in conoid tubercle morphology among early hominins. In *Gorilla*, when present, the morphology of the conoid tubercle is often flange-like, though not as pronounced as seen in *Pan*. In *Pongo,* the morphology of the conoid tubercle closely resembles that of *Pan* in producing a flange on the posterior margin of the clavicle, though it often appears more tuberosity-like than is typical for chimpanzees. Gibbons similarly have a conoid tubercle that broadly resembles that of chimpanzees in morphology. The apparent relationship of a flange-like conoid tubercle morphology with suspensory ape species suggests locomotor repertoire may play a role in the expression of this feature although there might also be a phylogenetic signal. The diversity of conoid tubercle morphology within fossil and extant hominids suggest that the functional significance of this trait is unclear and that caution is necessary before making functional inferences in relation to fossil species based on this feature.

Clavicular Nutrient Foramina

U.W. 102a-021 exhibits a nutrient foramen located at the boundary between the inferior surface and posterior margin on the acromial one-third of the clavicle. Site 101/the Dinaledi chamber preserves numerous clavicular remains attributed to *H. naledi* displaying similar nutrient foramina—U.W. 101-1229, U.W. 101-1503, U.W. 101-1347, and U.W. 101-1083 (Feuerriegel et al. 2017). The positioning of this foramen on both the U.W. 101-1347 and U.W. 102a-021 claviculae is similar to the modern human condition, with nutrient foramina located on the posterior part of the subclavian sulcus in the acromial one-third of the clavicle (Voisin 2012). The nutrient foramina of U.W. 101-1083 and U.W. 101-258 claviculae are on the superior surface, which differs from what is usually seen in modern humans, and is well outside the *P. troglodytes* and *Gorilla* distribution. Nutrient foramen position in *P. troglodytes* is unique, with foramina located on the posterior border of the clavicle and close to the sternal end. In *Gorilla*, there are most often two or three nutrient foramina randomly distributed on the clavicular diaphysis. Two claviculae from the Dinaledi chamber display two foramina—U.W. 101-1229 and U.W. 101-1503 (Feuerriegel et al. 2017). As U.W. 101-1229 is considered to be a young adult (Feuerriegel et al. 2017), the high number of foramina is unusual because the number of nutrient foramina seems to increase with age, at least in modern humans (Voisin 2012). The developmental stage of

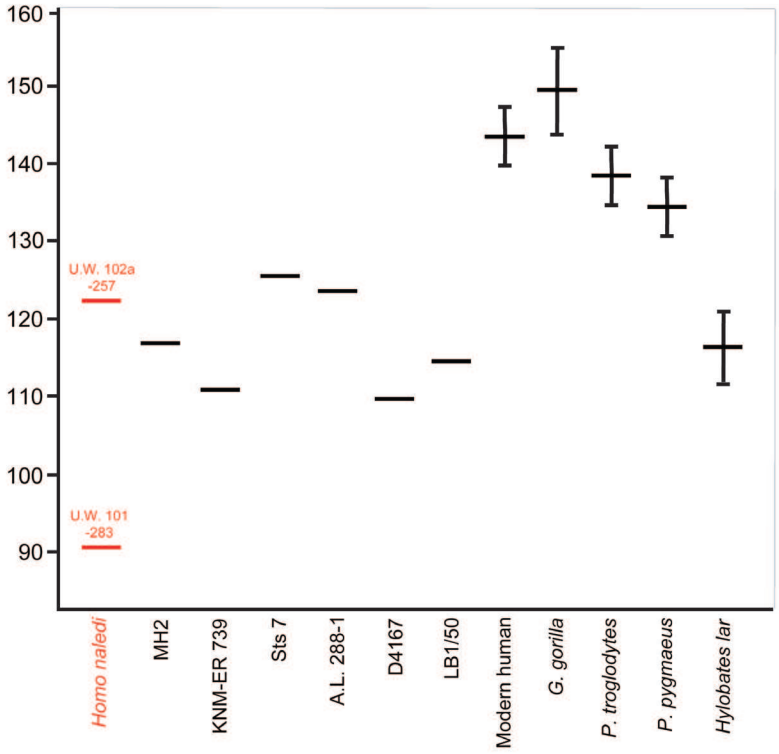

Figure 13. Mean adult humeral torsion values in degrees and standard deviation in extant and extinct hominids. Refer to Table 11 for information on specific values and samples.

U.W. 101-1503 is unknown.

HUMERAL COMPARISONS

Humeral Torsion

Using Larson's (1996) regression formulae, humeral torsion in U.W. 102a-257 is estimated at 120.1° when using head size as the single-variable best predictor of torsion (Figure 13; Table 11). When using the suite of proximal humeral features used to estimate humeral torsion in Sts 7, torsion is predicted as 126.2°. The values for U.W. 102a-257 humerus in the Sts 7 equation are 123° supraspinatus-infraspinatus facet angle, 7.8mm subscapularis facet width, and 31° infraspinatus facet angle. The mean of the two torsion estimates is 123.1°.

Proximal Humeral 3D Geometric Morphometrics

The first three PCs explained 62.9% of the variance in the sample (PC1=30.4%; PC2=19.5%; PC3=13.1%); the remaining PCs each explained <6% of the variance. A plot of PC1 against PC2 (Figure 14) shows clear differences between the groups, with only a slight overlap for the 95% equiprobability ellipses of group means for *P. troglodytes, P. pygmaeus,* and *Hylobates* sp.; *Macaca* sp., *G. gorilla*, and *H. sapiens* are well-differentiated. PC3 does not differentiate between the groups.

Principal Component 1 distinguished hominoid taxa from cercopithecoid taxa. *Macaca* sp. falls on the negative end of the axis, whereas *G. gorilla* and *P. pygmaeus* fall on the positive end. *Homo sapiens, Hylobates* sp., and *P. troglodytes* form a cluster and disperse around zero for PC1, with *Hylobates* and *Pan* occupying the most intermediate position on the plot, hovering around zero for both PC1 and PC2. While PC1 clearly differentiates *Macaca* sp. from the hominoids, it does a poor job of distinguishing within the hominoids, extant and fossil species alike; only *Hylobates* and *Pongo* distinguish well from each other.

Wireframe graphs were generated to visualize shape changes along the principal components (Figure 15). Shape changes toward the positive end of the PC1 axis (towards the hominoids) are driven by humeral heads that are more medially-oriented with an enlarged articular surface, a less projecting greater tubercle, a cranially-oriented *m. infraspinatus* insertion, a more laterally-oriented lesser tubercle with lateral expansion of the insertion for *m. subscapularis*, and a narrower bicipital groove. Shape changes toward the negative end of the PC1 axis are instead driven by a more posteriorly-oriented humeral head, large tubercles relative to the articular surface, a more anteriorly-oriented lesser tubercle, and a shallower and wider bicipital groove.

For PC2, *H. sapiens* exhibits the most negative scores of all species examined and is well-differentiated from other taxa, whereas the most terrestrial quadruped species, *Macaca* sp. and *G. gorilla,* exhibit the most positive values. While the more arboreal apes form a relatively distinct group intermediate to the *Gorilla-Macaca* cluster and *H. sapiens*, PC2 does a better job distinguishing *Pan* from gibbons and orang-utans, with *Hylobates* and *Pongo* exhibit more nega-

TABLE 11. HUMERAL TORSION VALUES (degrees) IN *HOMO NALEDI*, OTHER FOSSIL HOMININS, AND EXTANT HOMINOIDS.*

Species	Mature	Immature
Homo naledi (U.W. 101-283)	91.0°	-
Homo naledi (U.W. 101-948)	-	105.0°
Homo naledi (U.W. 102a-257)	123.1°	-
H. erectus (KNM WT15000)[a]	-	111.5°
H. erectus (D4167)[b]	110.0°	-
H. erectus (D2680)[b]	-	104.0°
H. floresiensis (LB1)[a]	115.0°	-
A. sediba (MH1)[c]	-	112.0°
A. sediba (MH2)[c]	117.0°	-
A. afarensis (A.L. 288-1)[d]	124.0°	-
A. africanus (STS7)[d]	126.0°	-
A. boisei (KNM-ER 739)[d]	111.0°	-
H. sapiens[e]	144.1° (SD 6.5°, n=20)	137.1° (SD 8.5°, n=50)
P. troglodytes[f]	139.0° (SD 6.7°, n=7)	136.4° (SD 13.3°, n=44)
G. gorilla[f]	150.0° (SD 9.8°, n=5)	152.3° (SD 12.1°, n=44)
P. pygmaeus/abelii[e]	135.0° (SD 6.5°, n=5)	138.4° (SD 7.5°, n=9)
H. lar[e]	116.6° (SD 8.1°, n=11)	118.0° (SD 6.9°, n=10)

Standard deviation values are presented in parentheses for the extant groups. See text for a discussion of these values for *H. naledi.*

[a]Data from Larson et al. (2007).

[b]Data from Lordkipanidze et al. (2007).

[c]Data from Churchill et al. (2013).

[d]Data from Larson (Larson, 1996).

[e]Collected from specimens at the Raymond A. Dart Collection, University of Witwatersrand, South Africa.

[f]Collected from specimens at the American Museum of Natural History, Cleveland Museum of Natural History, and Anthropological Institute & Museum, University of Zürich.

tive values than *Pan*. Shape change toward the positive side of the PC2 axis (toward the more terrestrial quadrupeds; see Figure 15) are driven by articular surfaces with more spherical contours when viewed anteriorly with a point of maximum convexity that is located more medially and superiorly. The lesser tubercle/*m. subscapularis* insertion has a more proximodistal orientation, while the greater tubercle projects somewhat more above the humeral head than previously described, situating the *m. supraspinatus* insertion more cranially, the *m. teres minor* insertion more laterally, and the *m. infraspinatus* insertion more posteriorly with a more proximodistal orientation. Shape change toward the negative side of the PC2 axis is characterized by articular surfaces that are flatter superiorly with a more distal point of maximum convexity and elliptical articular contour. The greater tubercle does not project past the articular surface, and the supraspinatus insertion facet is proportionally smaller with a more anterior tilt rather than facing more cranially as seen on the positive end of the PC2 axis. Similarly, the infraspinatus insertion facet is oriented more cranially relative to its shape on the positive end of the PC. The *m. teres minor* insertion is positioned more posteriorly. The lesser tubercle is obliquely oriented relative to the positive end of the axis.

In terms of the fossil specimens, most of the fossil humeri exhibit negative scores close to zero on PC1 (barring Regourdou 1, attributed to *H. neanderthalensis*, which has a positive score) and fall outside the convex hulls for the extant hominoids. A.L. 288-1aml (*A. afarensis*) exhibits a slightly more negative value than the lower extreme of the distribution of *H. sapiens* on PC1; Omo 119-73-2817 (*Australopithecus* sp.) and MH2 (*A. sediba*) fall at the lower margin of distribution of both *Hylobates* sp. and *H. sapiens.* U.W. 102a-257 (*H. naledi*) is intermediate for modern humans on PC1 and falls in the negative range of scores for *Pan.* The Regourdou 1 humerus exhibits the most positive scores on PC1 of any of the fossil material, falling within the upper extreme of scores for *H. sapiens*, but overlapping with *Pongo* and *Pan.* The fossil material separates more cleanly along PC2. *H. naledi* exhibits the most positive values of the fossil specimens for this component, falling squarely within the range of *Pan* and the upper range of the scores of *Pongo* and *Hylobates.* The australopith material clusters with *Pongo* and *Hylobates*, with A.L. 288-1aml falling closer to the lower edge of the values of *Pan* than the other two specimens; Omo 119-73-2817 falls within the overlapping zone of *H.*

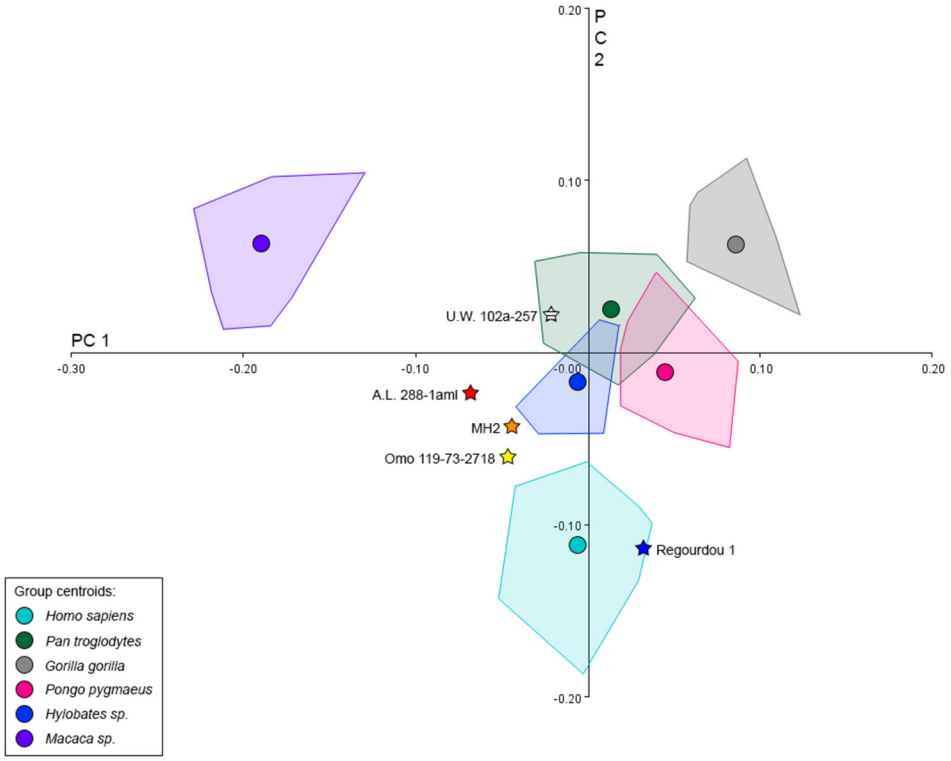

Figure 14. Plot of PC1 and PC2 for the proximal humeral 3D geometric morphometric PCA. Fossil hominin specimens are denoted by stars.

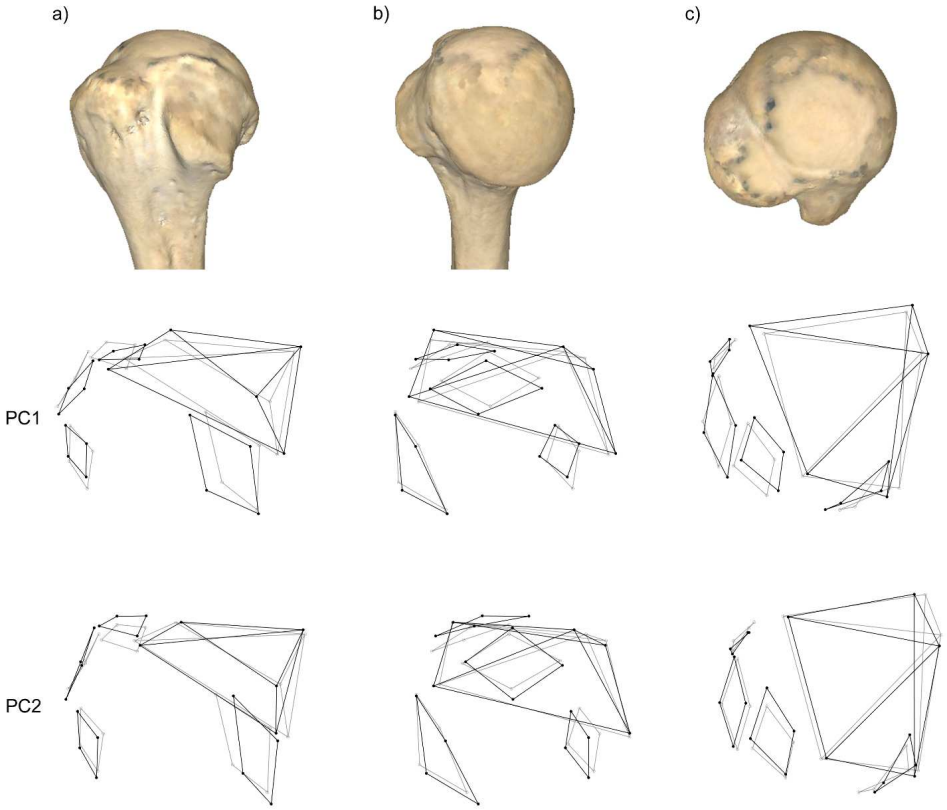

Figure 15. Wireframe shape changes for PC1 and PC2 of the proximal humeral geometric morphometric analysis in three anatomical views. **a)** *Anterolateral, showing the bicipital groove and tubercles;* **b)** *anteromedial, showing the articular surface and lesser tubercle; and* **c)** *superior view. Grey wireframes denote the shape change at the negative end of the distribution along the PC axis, whereas black wireframes denote the shape change at the positive end of the distribution along the PC axis.*

TABLE 12. EIGENVALUES AND EIGENVECTORS FROM THE ULNAR PRINCIPAL COMPONENTS ANALYSIS.

Component Number	Eigenvalue	Percentage Variance Explained
1	2.5270	31.587
2	1.5826	19.782
3	1.2247	15.309
4	1.0829	13.536
5	0.8212	10.265
6	0.4242	5.303
7	0.3374	4.218

Eigenvectors	PC 1	PC 2	PC 3	PC 4
TAP	0.38895	0.49103	-0.03533	0.18703
CHT	0.30804	0.50870	0.34991	-0.15181
OAP	0.28482	0.02108	-0.78672	0.18190
TL	0.23704	-0.34708	0.25133	-0.67261
TP	0.38583	-0.43067	0.14899	0.15820
OL	-0.48041	0.03085	-0.44991	-0.33106
PAP	-0.43577	0.34351	0.31072	0.00129
PTV	-0.21671	-0.27347	0.31273	0.63621

sapiens and *P. pygmaeus*. *H. neanderthalensis* (Regourdou 1) falls within the modern human group for PC2.

ULNAR COMPARISONS

The first four PCs had eigenvalues greater than 1 (Table 12) and were thus retained. These components combined to account for roughly 80% of the variation observed in the dataset. The first PC explains 31.6% of the total variance, and largely contrasts trochlear AP diameter (TAP), tuberosity position (TP), and coronoid height (CHT) with olecranon length (OL) and proximal AP diameter (PAP) (see Table 12). Although Neandertals, with longer olecranon processes and AP-thicker proximal ulnar shafts, tend to have more negative scores on the component, PC1 overall does a poor job of distinguishing between groups (Figure 16). Principal component 2 represents 19.8% of the sample variation and serves to differentiate those individuals with a large TAP and CHT from those with high values of trochlear length (TL) and TP (see Table 12). As with PC1, groups are poorly separated along PC2 (see Figure 16), although Neandertals tend to have more negative values of this axis thanks to their having relatively (to modern humans) low trochlear AP diameters and distally positioned ulnar tuberosities (Churchill et al. 1996). When PC scores for PC1 and PC2 are plotted against one another (see Figure 16), LES 1 can be seen to fall within the distributions of all comparative groups except the australopiths, although it falls close to the margin of the australopith distribution. The Baringo ulna falls within the distributions of all groups except the early modern humans and is very close to the centroid of the australopith group.

The third PC accounts for 15.3% of the variance in the sample, and effectively contrasts CHT with olecranon AP diameter (OAP) and OL. This component tends to separate Neandertals and particularly australopiths, with tall and long olecranon processes, from modern humans (Figure 17). Both LES 1 and KNM-BK 66 have very negative scores on PC3, outside of the range of scores for all modern human groups and falling among the distributions of australopiths and Neandertals. Principal Component 4 represents 13.5% of the total sample variation, and effectively contrasts individuals with transversely wide proximal ulnar shafts (proximal transverse diameter; PTV) from individuals with great trochlear and olecranon lengths (TL and OL). Fossils groups are poorly separated along this axis (see Figure 17). Were it not for the inclusion of the OH 36 ulna (taxonomically uncertain, but possibly representing *P. boisei*), with its very broad AP proximal shaft and its relatively low trochlear length, into the australopith sample, the australopith distribution on PC4 would not exceed the range of values of the other groups on this axis. Both LES 1 and KNM-BK 66 fall within the range of PC scores of all the comparative groups on PC4. When the third and fourth PCs are considered together (see Figure 17), LES 1 and KNM-BK 66 can be seen to fall close to one another, although KNM-BK 66 falls within the australopith distribution (and very close to that group's centroid), while LES 1 falls outside of the ranges of PC scores of all the comparative groups (although closest to the australopith centroid: Table 13).

When the position of the LES 1 and KNM-BK 66 specimens relative to the other groups is examined in the shape space defined by all four principal components, they both

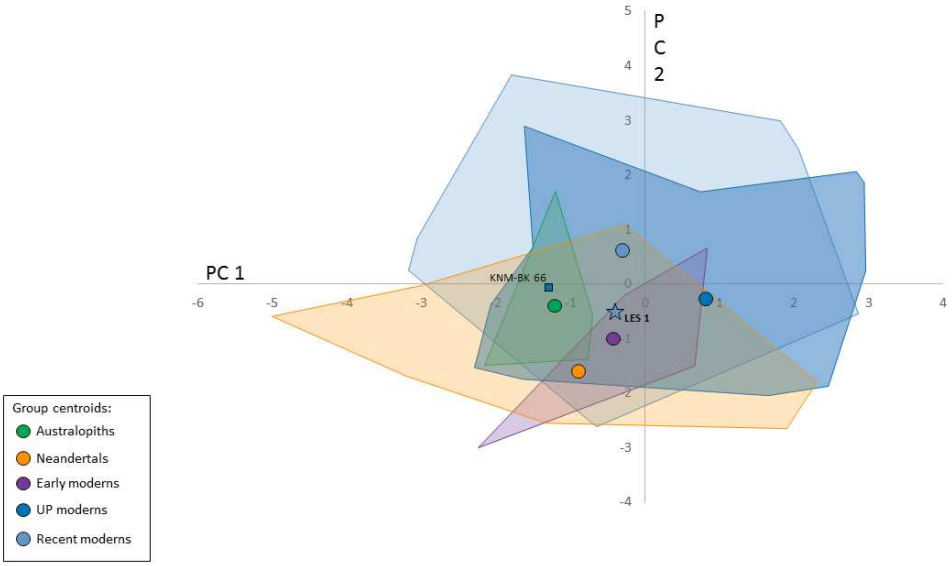

Figure 16. PC plot of ulna multivariate analysis of PC axes 1 and 2. For the sake of clarity, each comparative group is represented by the outline enclosing its individual data points and by group centroids (green: australopiths; orange: Neandertals; purple: early modern humans; dark blue: Upper Paleolithic modern humans; light blue: recent modern humans). The KNM-BK 68 and the LES 1 ulna data points have been added to the plot for comparative purposes (see text). PC1 represents 31.6% of the sample variance and PC2 represents 19.8% of the sample variance.

followed the identical pattern, being closest to the australopith centroid, followed by those of the Neandertal, early modern human, recent modern human, and Upper Paleolithic samples respectively (see Tables 12 and 13). The position of the LES 1 ulna differed significantly from only two comparative groups—Upper Paleolithic and recent modern humans. The Baringo ulna differed only from the Upper Paleolithic sample (see Table 13). In addition to the comparison between LES 1 and KNM-BK 66, it is also interesting to compare LES 1 with the proximal ulna recovered from the SAS Member of Klasies River Mouth (Churchill et al. 1996; Rightmire and Deacon 1991), given their geographic and temporal proximity (see Deacon 1989; Deacon and Geleijnse 1988; Dirks et al. 2017). On each principal component, the Klasies River Mouth (KRM) ulna fell among the distribution of scores of both Neandertals and later (Upper Paleolithic and recent) modern humans, reflecting its overall primitive morphology for the genus *Homo* (Churchill et al.

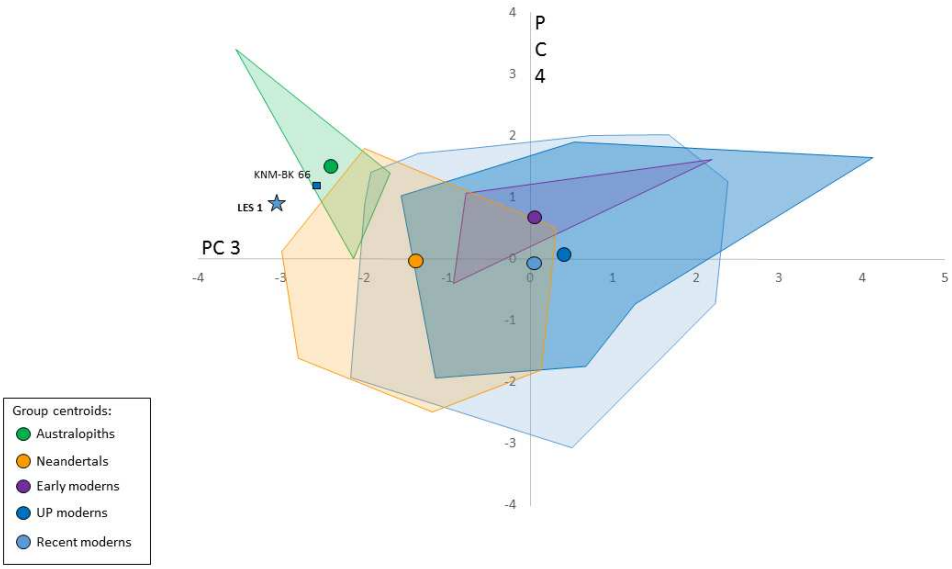

Figure 17. PC plot of ulna multivariate analysis of PC axes 3 and 4. Refer to the caption of Figure 16 for the color key. PC3 represents 15.3% of the sample variance and PC4 represents 13.5% of the sample variance.

TABLE 13. Z-SCORES OF EUCLIDEAN DISTANCES BETWEEN FOSSILS AND CENTROIDS OF COMPARATIVE GROUPS RELATIVE TO MEAN EUCLIDEAN DISTANCES WITHIN EACH GROUP.

	LES 1		KNM-BK 66	
	Z	*p*	*Z*	*p*
Australopiths	-0.7211	0.2355	0.2905	0.3857
Neandertals	0.9450	0.1723	0.9792	0.1637
Early Modern Humans	1.4250	0.0771	1.3618	0.0866
Upper Paleolithic Modern Humans	2.1142	**0.0173**	2.1340	**0.0164**
Recent Modern Humans	2.0120	**0.0221**	1.8549	0.3181

Values in **bold** are significant at Bonferroni-adjusted alpha of 0.025.

1996). The KRM ulna was primarily separated from LES 1 on the second and third PCs (Figure 18). In the space defined by these two components, the KRM ulna fell among the Neandertal specimens (although close to the margins of the Upper Paleolithic and recent modern human distributions), and closer to the Neandertal centroid than those of any of the modern human samples (including its own early modern human group). On these two axes, LES 1 fell outside of the distributions of all the comparative groups, although very close to both the australopith and Neandertal distribution boundaries (see Figure 18). When all four components are considered simultaneously, the KRM ulna fell very close to the centroid of its own sample (which includes the ulnae from Skhul and Qafzeh caves), whereas the LES 1 ulna was closest to the australopith centroid.

U.W. 102a-015/020 yielded an estimated trochlear notch orientation value of 14° using the method devised by Haile-Selassie et al. (2010) (Figure 19a; see Table 3). As this is likely to be an overestimation of trochlear notch angle, this estimate should be considered tentative as the real value may be somewhat lower. Regardless of the real value, this estimated orientation angle indicates that the trochlear notch of *H. naledi* is anteriorly oriented, similar to the condition suggested for all fossil hominin species (Drapeau et al. 2005). Olecranon height in U.W. 102a-015/020 similarly fell within the range of variation of australopith ulnae, and within the upper extremes of modern human and *Pan* variation (Figure 19b).

DISCUSSION

The claviculae of *H. naledi* display several derived and primitive characteristics in a unique configuration (Table 14). The results of these analyses indicate that, in superior view, the claviculae of *H. naledi* display somewhat diminished sigmoid curvature relative to that of modern humans and other fossil claviculae, and appear absolutely shorter than claviculae of *H. sapiens*. Nevertheless, *H. naledi* displays two distinct curvatures in this view, with an exter-

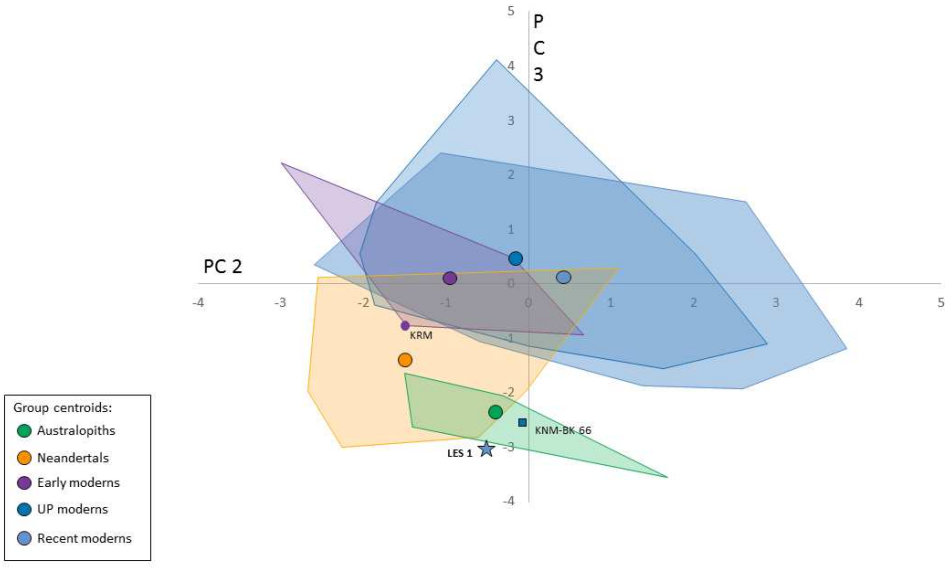

Figure 18. PC plot of ulna multivariate analysis of PC axes 2 and 3. Refer to the caption of Figure 16 for the color key. PC2 represents 19.8% of the sample variance and PC3 represents 15.3% of the sample variance.

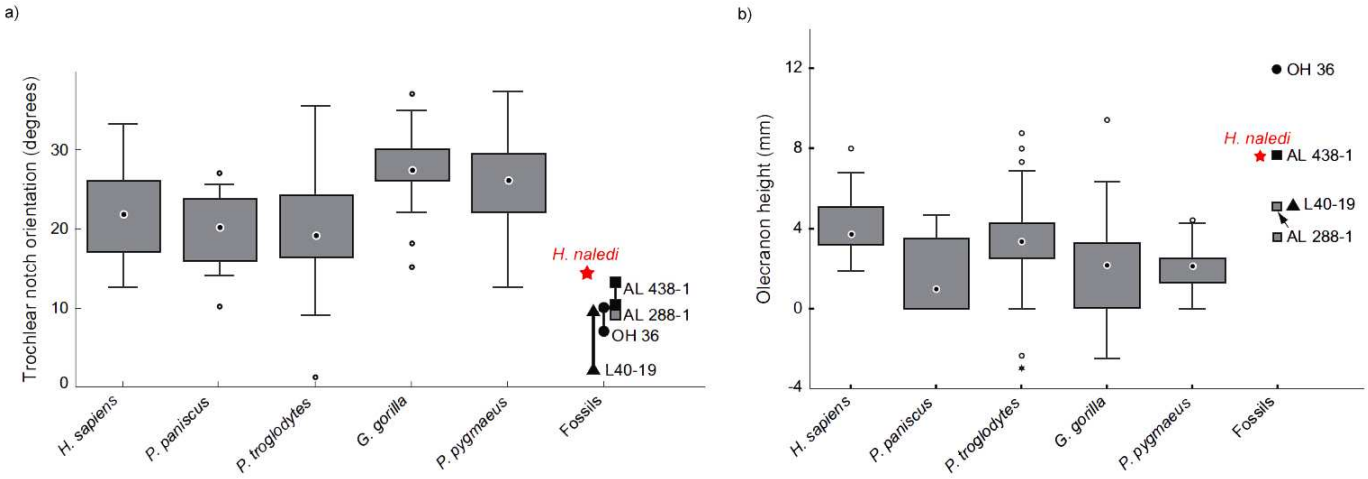

Figure 19. Ulnar metrical comparisons. **a)** *Trochlear notch orientation (in degrees) and* **b)** *olecranon process height (in mm) in fossil and extant samples. Trochlear notch orientation was estimated on U.W. 102a-015/020; refer to main text for a discussion of this value. Fossil hominins have trochlear notches that are oriented more anteriorly than modern humans or extant apes (figure modified from Drapeau et al. [2005]).*

nal curvature slightly more pronounced than the internal curvature, conforming to a basically *Pan*-like pattern of diminished sigmoid curvature relative to modern humans (Voisin 2006a). Voisin (2000, 2006a, b) attributed a sigmoid shape as one promoting efficient arm elevation and protraction, with a pronounced internal curvature increasing the lever arm of *M. pectoralis major*. While the increase in curvature provides increased mechanical leverage to the upper limb from the shoulder musculature, it also has the effect of increasing the weakness of the clavicle when exposed to bending and torsional forces at the junction of the two curvatures (Harrington et al. 1993; Mays et al. 1999). The less pronounced sigmoid curvature of the *H. naledi* clavicle implies a stronger clavicle than typifies modern humans. As the clavicle provides the only major strut of force transference/diffusion from the upper limb to the axial skeleton (Harrington et al. 1993; Mays et al. 1999), it is probable that *H. naledi* was using its upper limb to some degree in locomotor behavior, with a clavicle adapted to diffusing pronounced flexion or torsional forces in the upper limb.

An ape-like interpretation of clavicular curvature morphology is reinforced in posterior view by the presence of two pronounced curvatures in U.W. 102a-021. *Homo naledi* had claviculae with both inferior and superior curvatures in this view, fitting with the distribution known for *Pan*. Claviculae with this shape are more obliquely oriented and articulate with a scapula positioned high on the thorax (Voisin 2004, 2006a, b). *H. naledi* aligns closely with highly arboreal species such as *Pan*. Clavicular morphology in posterior view has been argued to define scapula position with regard to the thorax, and Voisin (2010) has suggested three distinct shoulder configurations within the genus *Homo* (see Table 8). Scapula position on the thorax depends greatly on clavicle length and morphology of the

TABLE 14. TABLE SUMMARZING THE HUMAN AND NON-HUMAN CHARACTRERS OF THE U.W. 102a-021 CLAVICLE (*Homo naledi*).

Human Traits	Non-Human Traits
-	Short clavicle length
-	Low perimeter
-	High robustness
Presence of the subclavian sulcus	-
Presence and morphology of the rhomboid facet	-
Nutriment foramina frequently on the posterior part of the subclavius sulcus, in the acromial on third	Frequent duplication of the nutriment foramina
-	Curvatures in superior view (like *Pan*)
-	Curvatures in posterior view (like living great apes)

thorax (Voisin 2006a, 2010; Chan 2007; Larson 2007; but see Roach and Richmond 2015 for an alternative view). Though there is very little information available concerning *H. naledi* thoracic form, it has been inferred that the thorax was more ape-like than human-like in this species (Williams et al. 2017). *H. naledi*'s clavicular curvatures in posterior view are consistent with Voisin's Group 1a, characterized by a relatively short clavicle and a scapula that is positioned high and somewhat laterally rotated about the thorax (see Table 8). This is a primitive configuration relative to the derived, long-and-low shoulder position that characterizes modern humans and later populations of fossil hominins (e.g., early and recent modern human populations; Larson 2007). The Dinaledi Chamber preserves one partial scapula, U.W. 101-1301, with bar-glenoid and axillary border/spine angles indicative of a markedly cranially-oriented glenoid fossa and very oblique scapular spine, respectively (Feuerriegel et al. 2017). This scapula configuration is similar to what is seen in *Hylobates* and *Pan*, and is inferred to reflect the habitually overhead posture of the arm in suspensory apes to assist with efficient arm elevation. The markedly ape-like configuration of the scapula from the Dinaledi assemblage is congruent with the ape-like clavicular curvatures of the LES 1 individual.

The robusticity of U.W. 102a-021 falls within the highest values for modern human and early modern human claviculae, and within the range of variation for australopiths, *Pan*, and *Gorilla* (see Figure 10). Within the extant hominoids generally, the most gracile claviculae belong to modern humans, increasing in robusticity through *P. troglodytes*, and reaching the greatest level of robusticity with *Gorilla*. *Pongo pygmaeus* has the greatest degree of variation for robusticity index, ranging across the variation seen in the three other hominoid species. The relative gracility of modern, Neandertal, and early *Homo* claviculae (e.g., KNM-WT 15000, OH 48, ATD 6-50, and A63) could be due to the habitually pendant position and peculiar function of the upper limb in manipulation rather than locomotion, though it should be noted that the extreme length of the Neandertal claviculae may have a confounding effect on this measurement for that taxon (Trinkaus 1983). On the other hand, elongation of the upper limb elements—and especially the clavicle—in gibbons (Kagaya et al. 2010) may also explain the markedly low robusticity index observed by Schultz (1930). The greater clavicular robusticity of *Australopithecus* and *H. naledi* likely reflects continued use of the upper limb in climbing behavior as an important part of their locomotor repertoire, and the need to buttress against high mechanical loading through the major axis of the clavicle.

Despite the notably primitive clavicular shape and robusticity, the costo-clavicular ligament facet of U.W. 102a-021 is human-like in morphology. All great apes possess a distinct and individualized costo-clavicular ligament like *H. sapiens* (Cave 1961), however, the morphology of this ligament varies between these groups, with a cylindrical or conical one in modern humans and a narrower, less cylindrical ligament in apes (Cave 1961). Moreover, all hominins, from *H. habilis* to modern humans, appear to exhibit a costo-clavicular ligament facet. Nevertheless, small sample sizes and limited reporting in the literature prohibit estimating the frequency in most fossil populations. In Neandertals, at least, the frequency of this trait is slightly lower than in modern humans (see Figure 10). The development of a depression-like rhomboid facet has been linked to the morphology of the costo-clavicular ligament, but may also be influenced by mechanical load, at least in modern humans (Jit and Kaur 1986; Paraskevas et al. 2009; Voisin 2012), and thus linked to upper limb function. The presence of a large, rugose costo-clavicular ligament facet in U.W. 102a-021 indicates that *H. naledi* likely had a human-like costo-clavicular ligament. In other words, the presence of the rhomboid facet and its human-like morphology in U.W. 102a-021 can be interpreted as a human-like characteristic. This may indicate that a cylindrical or conical costo-clavicular ligament shape is a synapomorphic trait for the genus *Homo*. What differentiates *H. naledi* from other *Homo* species is the expansion of a part of the rhomboid facet from the inferior surface onto the posterior surface of the sternal clavicle. The aetiology of this feature in U.W. 102a-021 is unclear.

The function of the costo-clavicular ligament is still much-debated; very few studies of the sternoclavicular joint have been conducted, even in modern humans, possibly due to its very low incidence of pathology (Bearn 1967; Cave 1961; Negri et al. 2014; Spencer et al. 2002; Tubbs et al. 2009) and the fact that the sternoclavicular joint is the least constrained joint in humans (Spencer et al. 2002). For some individuals, the costo-clavicular ligament has nearly no role in clavicular support (Bearn 1967; Spencer et al. 2002), whereas for others, it is one of the major structures stabilizing the sternoclavicular joint (Negri et al. 2014; Tubbs et al. 2009). Nevertheless, more recent studies have demonstrated that the costo-clavicular ligament is essential in preventing the dislocation of the sternoclavicular joint when the clavicle is elevated or retracted, but has a limited function during protraction (Negri et al. 2014; Tubbs et al. 2009). A large rhomboid facet in *H. naledi* likely reflects hypertrophy of the costo-clavicular ligament to stabilize against increased intra-articular stresses at the sternoclavicular joint, indicating regular elevation and powerful flexion of the humerus, as would be expected in climbing behavior.

The humeral morphology of LES 1/U.W. 102a-257 agrees well with what is known of the proximal humerus from the Dinaledi Chamber. Both U.W. 102a-257 and U.W. 101-283 display prominent lesser tubercles, a deep, narrow bicipital groove, and relatively smooth muscle attachments for some aspects of the shoulder musculature. Humeral torsion in LES 1, however, appears markedly greater than that previously documented for the largely-complete humerus, U.W. 101-283 (Feuerriegel et al. 2017). While Larson's (1996) regression formulae were designed for use on incomplete humeri, the landmarks necessary for their implementation on the proximal portion of U.W. 101-283 (humeral head, the greater tubercle/insertion facets for *mm. supraspinatus* and *infraspinatus*) are missing or not sufficiently intact. Torsion

in the Dinaledi humerus was instead estimated directly on surface scans using a set of alternative landmarks similar to those used by Churchill et al. (2013) to determine torsion in *A. sediba*. As such, the torsion values for the Lesedi material and the Dinaledi material are not directly comparable. The torsion values for U.W. 102a-257 fall more agreeably within the range of variation determined by Larson (1996) and others for fossil hominin humeri (see Table 11, see Figure 13), indicating that low humeral torsion is the primitive condition for hominins. If the torsion value for U.W. 101-283 is indeed correct and not an underestimate, it is possible that this humeral specimen is pathological or there is greater developmental plasticity in this feature in *H. naledi* than is currently recognized for other species. Further radiological investigation is required to shed light on the Dinaledi humeral specimen. Nevertheless, *H. naledi* maintains low humeral torsion and this, in combination with the primitive clavicular, proximal humeral, and thoracic (Williams et al. 2017) morphology supports previous interpretations of the *H. naledi* scapula as being situated high and possibly rotated somewhat laterally about the upper thorax (Feuerriegel et al. 2017), as previously suggested for KNM-WT 15000 and the Dmanisi hominins (Larson 2013), and *A. sediba* (Churchill et al. 2013), though the relative length of the *H. naledi* claviculae remains unknown.

Three-dimensional geometric morphometric analysis of the LES 1 humerus demonstrates that proximal humeral morphology in *H. naledi*, while sharing clear affinities with the arboreal apes *Pan* and *Hylobates*, maintains similarities with modern humans. LES 1 shares with *Pan* and *Pongo* an articular surface that is more spherical in contour with a superior aspect that is high and round, rather than low and flattened with an elliptical contour as in modern humans. Unlike *Pan, Gorilla*, and *Pongo*, *H. naledi* has a more posteriorly-oriented humeral head more similar to hylobatids and the lower ranges for modern humans. The tubercles are large relative to the articular surface, with greater tubercle insertions that are more ape-like than human-like in their shape and orientation. The lesser tubercle is more mosaic—it is anteriorly-facing, which is a more human-like feature, but with a proximodistal orientation to the subscapularis insertion facet that is more like arboreal apes (e.g., *Pan, Pongo,* and *Hylobates*). Overall, the proximal humeral shape of *H. naledi* more closely resembles the chimpanzee morphotype, according with the markedly ape-like partial scapula from the Dinaledi Chamber (Feuerriegel et al. 2017) and the primitive curvatures of the Lesedi clavicle. Collectively, these features speak to a highly mobile glenohumeral joint with an enhanced range of external rotation and circumduction (Larson 1995). The high and round articular surface in arboreal apes and *H. naledi*, coupled with a cranially-oriented scapular glenoid, is functionally related to overhead reaching and hanging behaviors—it permits stable articular contact between the humeral head and glenoid through the central and superior portions of the articular surface in greater ranges of arm abduction (Arias-Martorell et al. 2015b).

Moreover, the lateral orientation of the *teres minor* insertion on the greater tubercle in U.W. 102a-257 also speaks to an enhanced facility for external rotation/overhead reaching behaviors in *H. naledi*, conferring greater mechanical advantage to *m. teres minor* in its role as an external rotator (Arias-Martorell et al. 2015a). Larson (1995) has suggested that the orientations of the supra- and infraspinatus insertion facets relative to one another can be similarly informative about the functional morphology of the primate humerus. Apes are characterized by more cranially-oriented infraspinatus insertion facets relative to ceboids and cercopithecoids, indicating a component of abduction to the action of the infraspinatus muscle (Larson 1995; Larson and Stern 1986). Thus, the greater the frequency of arm raising and overhead forelimb postures in the locomotor repertoire of the species, the more cranial the orientation of the infraspinatus facet. Contrary to expectations, *H. naledi* is characterized by an infraspinatus facet that is more laterally-oriented. Nevertheless, Larson notes that hylobatids, the most suspensory hominoid species, do not fit this pattern and suggested instead that the very low degree of humeral torsion in *Hylobates* reduces the role of infraspinatus in arm-raising. In effect, the more lateral infraspinatus facet orientation in hylobatids reflects a diminished recruitment of the infraspinatus muscle in an arm-raising capacity and a greater recruitment of the subscapularis muscle instead to overcome the extreme lateral set to the elbow conferred by the very low humeral torsion. It is possible that a similar interpretation of infraspinatus facet orientation may be applied to *H. naledi*.

Interestingly, based on the GMM analysis, *H. naledi* appears more arboreal in its proximal humeral morphology than any of the australopith samples included in the analysis, despite being more derived in terms of its lower limb anatomy when compared to the lower limbs of *A. afarensis* and *A. sediba* (Harcourt-Smith et al. 2015; Marchi et al. 2017). A.L. 288-1aml, MH2/U.W. 88-57, and Omo 119-73-2718 all fall somewhat intermediate to *H. sapiens* and the *Pan-Pongo-Hylobates* cluster on PC2, and at the lower range of variation for hominoids along PC1. With respect to their position along PC1, the australopith humeri are broadly similar in some aspects of morphology to *H. naledi*—more posteriorly-oriented humeral heads, large tubercles relative to the articular surface, and more anteriorly-oriented lesser tubercles. The australopith humeri differ notably in being characterized by articular surfaces that are flatter superiorly with a more distal point of maximum convexity and elliptical articular contour than *H. naledi*. The infraspinatus insertion facet is oriented more cranially and the *teres minor* insertion more posteriorly in A.L. 288-1aml, MH2/U.W. 88-57, and Omo 119-73-2718 relative to U.W. 102a-257. The evidence suggests that *Australopithecus* was approaching a more human-like proximal humeral morphology through increasing compromise between adaptations advantageous for climbing and manual manipulatory behaviors (Drapeau 2012). By contrast, climbing appears to be an integral component of the locomotor repertoire of *H. naledi*, such that *H. naledi* is more similar to arboreal apes in its proximal humeral morphology despite its status as a

member of the genus *Homo* and its relatively recent date at 236–335 ka (Dirks et al. 2017).

As with the shoulder girdle remains, the Lesedi ulnar material aligns with a broadly australopith pattern rather than a typical modern human pattern in most respects. In the multivariate analyses of proximal ulna form, LES 1 was found to differ significantly from recent modern humans, exhibiting an anteroposteriorly taller and proximodistally longer olecranon process than typifies modern humans, similar to australopiths. The Lesedi ulna falls close to the probable *H. erectus* ulna from Baringo, KNM-BK 66 (Solan and Day 1992). This is consistent with morphological similarity between *H. naledi* and *H. erectus* in other aspects of the skeleton (Berger et al. 2015; Hawks et al. 2017; Laird et al. 2017), assuming the Baringo specimen represents *H. erectus*. Surprisingly, the KNM-BK 66 ulna falls closer to the specimens in the australopith sample than does LES 1, though both ulnae tend to cluster more with australopiths and Neandertals than with modern humans.

Two additional measures of proximal ulnar morphology were able to be assessed—trochlear notch orientation and olecranon proximodistal height (Drapeau et al. 2005). The orientation of the trochlear notch in U.W. 102a-015/020 is estimated at 14°, indicating an anteriorly-oriented trochlear notch, and the olecranon height is estimated at 7.8mm (see Figure 18). This trochlear notch orientation is similar to other fossil hominins, including A.L. 288-1, KSD-VP-1/1a, A.L. 438-1, ARA-VP-6/500, and Neandertals, and has been suggested to be a derived condition of all fossil hominins (see Figure 19a) (Drapeau et al. 2005; Haile-Selassie et al. 2010). *Homo naledi* also closely resembles A.L. 438-1, A.L. 288-1, and L40-19 in having relatively long olecranon processes proximodistally, though there is overlap within hominoid taxa for this feature (see Figure 18b). Chimpanzees, modern humans, and bonobos all have more proximally-oriented trochlear notches, with gorillas and orang-utans exhibiting the most proximally-facing notches of all hominoids (Aiello et al. 1999; Drapeau et al. 2005). Trochlear notch orientation is also structurally related to the orientation of the olecranon process (Drapeau et al. 2005; Drapeau 2012). Both *A. afarensis* (Drapeau et al. 2005) and Neandertals (Churchill et al. 1996; Hambücken 1998) have anteriorly oriented trochlear notches with proximally directed olecranon processes. Given that *H. naledi* also appears to fit the derived proximal ulna morphology of other fossil hominins, this suggests that the olecranon process of *H. naledi* was similarly proximally directed. Functionally, a proximally-oriented olecranon process has been linked to habitual use of the arm in flexed postures (Drapeau 2004; Knussmann 1967; Trinkaus and Churchill 1988), and Drapeau (2005) has suggested that an anteriorly-oriented trochlear notch may reflect a greater frequency and duration of transarticular loading at the elbow joint during those flexed postures relative to modern humans. Additionally, ulnar specimens from the Dinaledi Chamber exhibit reduced ulnar styloid processes compared to modern humans and an enhanced ability for ulnar deviation of the hand at the wrist, a trait which has been suggested by Ward (2007) as an important adaptation to overhead reaching behaviors. Distal ulna specimens have yet to be recovered from the Lesedi Chamber, but it is probable that the LES 1 individual similarly displayed reduced ulnar styloid processes. The ulna of *H. naledi*, then, is primitive in morphology and may reflect adaptations to greater and more frequent loading of the elbow joint during elbow flexion as well as overhead reaching.

CONCLUSION

The recovery of new material from the Lesedi Chamber of the Rising Star cave system sheds further light on the upper limb morphology of *H. naledi* and provides a unique opportunity to investigate the locomotor repertoire of this species in greater detail. Functionally, the shoulder region of *H. naledi* fits within the pattern that characterizes the upper limb of *Australopithecus*, though it differs notably in a number of features. The LES clavicle exhibits an ape-like pattern of clavicular curvatures indicative of a strong emphasis on overhead reaching and climbing behaviors. The LES 1 humerus shares clear affinities with the arboreal apes *Pan* and *Hylobates*—more so even than most australopithecine humeri—in maintaining an articular surface that has a spherical contour with a superior aspect that is high and round, and a more posteriorly-oriented humeral head. The proximal ulna is primitive in morphology compared to modern humans, but aligns well with the morphology seen in other fossil specimens in exhibiting a proximally-oriented olecranon process and anteriorly-oriented trochlear notch.

The upper thorax of *H. naledi* is narrow (Williams et al. 2017) and the glenohumeral joint is cranially directed, much as inferred for *Australopithecus* (Green 2013; Green and Alemseged 2012; Schmid 1983; Stern and Susman 1983). The holotype of *H. naledi* (DH1) preserves a nearly complete adult right hand (Berger et al. 2015). Kivell et al. (2015) describe the hand as possessing many derived features of the palm, thumb, and wrist shared with both modern humans and Neandertals, but nonetheless maintaining morphological features typical of climbing behaviors. Thumb-to-finger proportions indicate that the thumb is long relative to the other digits, although the fingers themselves are long again relative to the palm and exhibit marked phalangeal curvature, more so than even that seen in australopiths (Kivell et al. 2015). Phalangeal curvature is biomechanically significant as it has been demonstrated to reduce the strain experienced by the hand in flexed-finger grasping postures because the curvatures align the bone with the joint reaction forces (Nguyen et al. 2014; Richmond 2007). Given the high degree of curvature exhibited by *H. naledi*, it is clear that the hand and fingers experienced strong loading during grasping typical of climbing or suspensory behaviors.

Overall, the picture formed by the *H. naledi* upper limb and hand morphology is a mosaic. The marked phalangeal curvature and primitive pectoral girdle morphology indicate that climbing behavior remained a substantial part of the locomotor repertoire for this species. Curiously, the morphology of the leg and foot of *H. naledi* is that of an obligate biped (Harcourt-Smith et al. 2015; Marchi et al.

2016). Corbetta (2005) has argued that the upper limb must be freed from the requirements of locomotion in order for complex manual manipulatory behaviors to develop. The presence of a sizeable complex of derived manual morphologies in the hand and an irrefutably bipedal lower limb in *H. naledi* might then suggest that the upper limb played little role in locomotion, and that the arboreal features of the hand and shoulder represent primitive retentions. On the other hand, reduced phalangeal curvature in one immature proximal phalanx from *H. naledi* negates this conclusion. Phalangeal curvature has been demonstrated by Richmond (1998, 2007) to be strongly influenced by mechanical loading during ontogeny such that curvature is a functional response of the bone to behavior. Thus, the manual (Kivell et al. 2015), scapular (Feuerriegel et al. 2017), clavicular, and humeral remains demonstrate continued relevance of forceful grasping and overhead reaching behaviors, and thus of climbing and/or suspension, in the locomotor repertoire of *H. naledi* well into skeletal maturity. In this respect, the morphology of *H. naledi* speaks to greater locomotor diversity in the genus *Homo* than has previously been understood. Given that *Homo naledi* was discovered in a cave system and that their presence within that system is potentially non-trivial (Dirks et al. 2015), rock climbing may have comprised a significant portion of this climbing behavior. The Lesedi Chamber is currently undated, but the similar preservation of the Lesedi material to the Dinaledi material (Dirks et al. 2017) implies a similarly recent depositional history for LES 1 from the same biological population represented by the Dinaledi remains (Hawks et al. 2017). The similarity of the *H. naledi* elbow and shoulder morphology to several species of australopiths implies stabilizing selection for traits favoring vertical climbing behaviors for at least one lineage within the genus *Homo.*

ACKNOWLEDGEMENTS

This work was supported by funding from the National Science Foundation, Wenner-Gren Foundation, and the Leakey Foundation. We are grateful to Prof. Eric Delson and Assistant Prof. Will Harcourt-Smith for sharing 3D surface scans of non-human primate humeral material for use in this study. EF would also like to thank Miguel Ochoa at the University of Washington for his assistance assembling the non-human primate skeletal sample used in this study. MH and SM were financially supported by Swiss National Science Foundation grants No 31003A_156299/1 and 31003A_176319.

REFERENCES

Aiello, L.C., Wood, B., Key, C., and Lewis, M. 1999. Morphological and taxonomic affinities of the Olduvai ulna (OH 36). *American Journal of Physical Anthropology* 109, 89–110.

Arias-Martorell, J., Potau, J.M., Bello-Hellegouarch, G., Pastor, J.F., and Pérez-Pérez, A. 2012. 3D geometric morphometric analysis of the proximal epiphysis of the hominoid humerus. *Journal of Anatomy* 221, 394–405.

Arias-Martorell, J., Potau, J.M., Bello-Hellegouarch, G., and Pérez-Pérez, A. 2015a. Like Father, Like Son: assessment of the morphological affinities of A.L. 288–1 (*A. afarensis*), Sts 7 (*A. africanus*) and Omo 119–73–2718 (*Australopithecus* sp.) through a three-dimensional shape analysis of the shoulder joint. *PLoS ONE* 10, 1–28.

Arias-Martorell, J., Tallman, M., Potau, J.M., Bello-Hellegouarch, G., and Pérez-Pérez, A. 2015b. Shape analysis of the proximal humerus in orthograde and semi-orthograde primates: correlates of suspensory behavior. *American Journal of Primatology* 77, 1-19.

Arsuaga, J.L., Martinez, I., Garcia, A., and Lorenzo, C. 1997. The Sima de los Huesos crania (Sierra de Atapuerca, Spain): a comparative study. *Journal of Human Evolution* 33, 219–281.

Bearn, J.G. 1967. Direct observations on the function of the capsule of the sternoclavicular joint in clavicular support. *Journal of Anatomy* 101, 159–170.

Berger, L.R., Hawks, J., de Ruiter, D.J., Churchill, S.E., Schmid, P., Delezene, L.K., Kivell, T.L., Garvin, H.M., Williams, S.A., DeSilva, J.M., Skinner, M.M., Musiba, C.M., Cameron, N., Holliday, T.W., Harcourt-Smith, W., Ackermann, R.R., Bastir, M., Bogin, B., Bolter, D., Brophy, J., Cofran, Z.D., Congdon, K.A., Deane, A.S., Dembo, M., Drapeau, M., Elliott, M.C., Feuerriegel, E.M., Garcia-Martinez, D., Green, D.J., Gurtov, A., Irish, J.D., Kruger, A., Laird, M.F., Marchi, D., Meyer, M.R., Nalla, S., Negash, E.W., Orr, C.M., Radovčić, D., Schroeder, L., Scott, J.E., Throckmorton, Z., Tocheri, M.W., VanSickle, C., Walker, C.S., Wei, P., and Zipfel, B. 2015. *Homo naledi*, a new species of the genus *Homo* from the Dinaledi Chamber, South Africa. *eLife* 4, e09560.

Bookstein, F.L. 1991. *Morphometric Tools for Landmark Data: Geometry and Biology*. Cambridge University Press, Cambridge, UK.

Carretero, J.M., Arsuaga, J.L., Lorenzo, C. 1997. Clavicles, scapulae and humeri from the Sima de los Huesos site (Sierra de Atapuerca, Spain). *Journal of Human Evolution* 33, 357–408.

Carretero, J.M., Lorenzo, C., Arsuaga, J.L. 1999. Axial and appendicular skeleton of *Homo antecessor. Journal of Human Evolution* 37, 459–499.

Cave, A.J.E. 1961. Nature and morphology of the costoclavicular ligament. *Journal of Anatomy* 95, 170–179.

Chan, L.K. 2007. Scapula position in primates. *Folia Primatologica* 78, 19–35.

Churchill, S.E. 1994. *Human Upper Body Evolution in the Eurasian Later Pleistocene*. Ph.D. Dissertation. University of New Mexico, Albuquerque.

Churchill, S.E., Holliday, T.W., Carlson, K.J., Jashashvili, T., Macias, M.E., Mathews, S., Sparling, T.L., Schmid, P., de Ruiter, D.J., and Berger, L.R. 2013. The upper limb of *Australopithecus sediba*. *Science* 340, 1233477.

Churchill, S.E., Pearson, O.M., Grine, F.E., Trinkaus, E., and Holliday, T.W. 1996. Morphological affinities of the proximal ulna from Klasies River main site: archaic or modern? *Journal of Human Evolution* 31, 213–237.

Churchill, S.E. and Trinkaus, E. 1990. Neandertal scapular glenoid morphology. *American Journal of Physical An-*

thropology 83, 147–160.

Corbetta, D., 2005. Dynamic interactions between posture, handedness, bimanual coordination in human infants: why stone knapping might be a uniquely hominin behaviour. In *Stone Knapping: The Necessary Conditions for a Uniquely Hominin Behaviour*, Roux, V. and Bril, B. (eds.). McDonald Institute for Archaeological Research, Cambridge, England, pp. 187–204.

Darroch, J.N. and Mosimann, J.E. 1985. Canonical and principal components of shape. *Biometrika* 72, 241–252.

Deacon, H.J. 1989. Late Pleistocene palaeoecology and archaeology in the southern Cape, South Africa. In *The Human Revolution*, Mellars, P.B. and Stringer, C.B. (eds.). Edinburgh University Press, Edinburgh, pp. 547–564.

Deacon, H.J. and Geleijnse, V.B. 1988. The stratigraphy and sedimentology of the Main Site sequence, Klasies River, South Africa. *South African Archaeological Bulletin* 43, 5–14.

Dembo, M., Radovčić, D., Garvin, H.M., Laird, M.F., Schroeder, L., Scott, J.E., Brophy, J., Ackermann, R.R., Musiba, C.M., de Ruiter, D.J., Mooers, A.Ø., and Collard, M. 2016. The evolutionary relationships and age of *Homo naledi*: an assessment using dated Bayesian phylogenetic methods. *Journal of Human Evolution* 97, 17–26.

Dirks, P.H., Berger, L.R., Roberts, E.M., Kramers, J.D., Hawks, J., Randolph-Quinney, P.S., Elliott, M., Musiba, C.M., Churchill, S.E., de Ruiter, D.J., Schmid, P., Backwell, L.R., Belyanin, G.A., Boshoff, P., Hunter, K.L., Feuerriegel, E.M., Gurtov, A., Harrison, J.d.G., Hunter, R., Kruger, A., Morris, H., Makhubela, T.V., Peixotto, B., and Tucker, S. 2015. Geological and taphonomic context for the new hominin species *Homo naledi* from the Dinaledi Chamber, South Africa. *eLife* 4, e09561.

Dirks, P.H.G.M., Roberts, E.M., Hilbert-Wolf, H., Kramers, J.D., Hawks, J., Dosseto, A., Duval, M., Elliott, M., Evans, M., Grün, R., Hellstrom, J., Herries, A.I.R., Joannes-Boyau, R., Makhubela, T.V., Placzek, C.J., Robbins, J., Spandler, C., Wiersma, J., Woodhead, J., and Berger, L.R. 2017. The age of *Homo naledi* and associated sediments in the Rising Star Cave, South Africa. eLife 6, e24231.

Drapeau, M.S., 2012. Forelimb adaptations in *Australopithecus afarensis*, in: Reynolds, S.C., Gallagher, A. (Eds.), *African Genesis: Perspectives on Human Evolution*. Cambridge University Press, Cambridge, pp. 223-247.

Drapeau, M.S.M. 2004. Functional anatomy of the olecranon process in hominoids and Plio-Pleistocene hominins. *American Journal of Physical Anthropology* 124, 297–314.

Drapeau, M.S.M. 2008. Articular morphology of the proximal ulna in extant and fossil hominoids and hominins. *Journal of Human Evolution* 55, 86–102.

Drapeau, M.S.M., Ward, C.V., Kimbel, W.H., Johanson, D.C., and Rak, Y. 2005. Associated cranial and forelimb remains attributed to *Australopithecus afarensis* from Hadar, Ethiopia. *Journal of Human Evolution* 48, 593–642.

Feuerriegel, E.M., Green, D.J., Walker, C.S., Schmid, P., Hawks, J., Berger, L.R., and Churchill, S.E. 2017. The upper limb of *Homo naledi*. *Journal of Human Evolution* 104, 155–173.

Green, D.J. 2013. Ontogeny of the hominoid scapula: the influence of locomotion on morphology. *American Journal of Physical Anthropology* 152, 239–260.

Green, D.J. and Alemseged, Z. 2012. *Australopithecus afarensis* scapular ontogeny, function, and the role of climbing in human evolution. *Science* 338, 514–517.

Haile-Selassie, Y., Latimer, B.M., Alene, M., Deino, A.L., Gibert, L., Melillo, S.M., Saylor, B.Z., Scott, G.R., and Lovejoy, C.O. 2010. An early *Australopithecus afarensis* postcranium from Woranso-Mille, Ethiopia. *Proceedings of the National Academy of Sciences USA* 107, 12121–12126.

Haile-Selassie, Y., Suwa, G., and White, T.D. 2009. Hominidae. In Ardipithecus kadabba: *Late Miocene evidence from the Middle Awash, Ethiopia*, Haile-Selassie, Y. and WoldeGabriel, G. (eds.), University of California Press, Berkely & Los Angeles, pp. 159–236.

Hambücken, A. 1998. Morphologie et fonction du coude et de l'avant-bras des néandertaliens. *Bulletin et* Mémoires de la Societé d'Anthropologie de Paris 10, 213–236.

Harcourt-Smith, W.E.H., Throckmorton, Z., Congdon, K.A., Zipfel, B., Deane, A.S., Drapeau, M.S.M., Churchill, S.E., Berger, L.R., and DeSilva, J.M. 2015. The foot of *Homo naledi*. *Nature Communications* 6, 1–8.

Harrington, M.A., Keller, T.S., Seiler, J.G., Weikert, D.R., Moeljanto, E., and Schwartz, H.S. 1993. Geometric properties and the predicted mechanical behavior of adult human clavicles. *Journal of Biomechanics* 26, 417–426.

Hawks, J., Elliott, M., Schmid, P., Churchill, S.E., Ruiter, D.J.d., Roberts, E.M., Hilbert-Wolf, H., Garvin, H.M., Williams, S.A., Delezene, L.K., Feuerriegel, E.M., Randolph-Quinney, P., Kivell, T.L., Laird, M.F., Tawane, G., DeSilva, J.M., Bailey, S.E., Brophy, J.K., Meyer, M.R., Skinner, M.M., Tocheri, M.W., VanSickle, C., Walker, C.S., Campbell, T.L., Kuhn, B., Kruger, A., Tucker, S., Gurtov, A., Hlophe, N., Hunter, R., Morris, H., Peixotto, B., Ramalepa, M., Rooyen, D.V., Tsikoane, M., Boshoff, P., Dirks, P.H.G.M., and Berger, L.R. 2017. New fossil remains of *Homo naledi* from the Lesedi Chamber, South Africa. *eLife* 6, e24232.

Jashashvili, T. 2005. *Hominid Upper limb Remains from the Palaeolithic site of Dmanisi, a Morphometric Comparison to Taxonomic Units and Functional Interpretation*. University of Ferrara, Republic of Georgia.

Jit, I. and Kaur, H. 1986. Rhomboid fossa in the clavicles of North Indians. *American Journal of Physical Anthropology* 70, 97–103.

Kagaya, M., Ogihara, N., and Nakatsukasa, M. 2010. Is the clavicle of apes long? An investigation of clavicular length in relation to body mass and upper thoracic width. *International Journal of Primatology* 31, 209–217.

Kappelman, J., Ketcham, R.A., Pearce, S., Todd, L., Akins, W., Colbert, M.W., Feseha, M., Maisano, J.A., and Witzel, A. 2016. Perimortem fractures in Lucy suggest mor-

tality from fall out of tall tree. *Nature* 537, 503–507.
Kivell, T.L., Deane, A.S., Tocheri, M.W., Orr, C.M., Schmid, P., Hawks, J., Berger, L.R., and Churchill, S.E. 2015. The hand of *Homo naledi*. *Nature Communications* 6, 1–9.
Klingenberg, C.P. 2011. MorphoJ: An integrated software package for geometric morphometrics. *Molecular Ecology Resources* 11, 353–357.
Knussmann, V.R. 1967. *Humerus, Ulna, und Radius der Simiae*. S. Krager, Basel.
Knussmann, R. 1988. *Anthropologie: Handbuch der vergleichenden Biologie des Menschen*. Zugleich 4. Auflage des Lehrbuchs der Anthropologie, begründet von Rudolf Martin. Stuttgart, Fischer.
Laird, M.F., Schroeder, L., Garvin, H.M., Scott, J.E., Dembo, M., Radovčić, D., Musiba, C.M., Ackermann, R.R., Schmid, P., Hawks, J., Berger, L.R., and de Ruiter, D.J. 2017. The skull of *Homo naledi*. *Journal of Human Evolution* 104, 100–123.
Larson, S.G. 1995. New characters for the functional interpretation of primate scapulae and proximal humeri. *American Journal of Physical Anthropology* 98, 13–35.
Larson, S.G. 1996. Estimating humeral torsion on incomplete fossil anthropoid humeri. *Journal of Human Evolution* 31, 239–258.
Larson, S.G. 2007. Evolutionary transformation of the hominin shoulder. *Evolutionary Anthropology* 16, 172–187.
Larson, S.G. 2013. Shoulder morphology in early hominin evolution. In *The Paleobiology of* Australopithecus, Reed, K.E., Fleagle, J.G., and Leakey, R.E. (eds.). Springer, Dordrecht, pp. 247–261.
Larson, S.G., Jungers, W.L., Morwood, M.J., Sutikna, T., Jatmiko, Saptomo, E.W., Due, R.A., and Djubiantono, T. 2007. *Homo floresiensis* and the evolution of the hominin shoulder. *Journal of Human Evolution* 53, 718–731.
Larson, S.G. and Stern, J.T. 1986. EMG of scapulohumeral muscles in the chimpanzee during reaching and "arboreal" locomotion. *American Journal of Anatomy* 176, 171–190.
Leakey, M., Tobias, P.V., Martyn, J.E., and Leakey, R.E.F. 1969. An Acheulian industry with prepared core technique and the discovery of a contemporary hominid mandible at Lake Baringo, Kenya. *Proceedings of the Prehistoric Society* 35, 48–76.
Leakey, R.E.F., Walker, A., Ward, C.V., and Grausz, H.M. 1989. A partial skeleton of a gracile hominid from the Upper Burgi Member of the Koobi Fora Formation, East Lake Turkana, Kenya. In *Hominidae: Proceedings of the 2nd International Congress of Human Paleontology, Turin*. Giacobini, G. (ed.). Jaka Books, Milan, pp. 167–173.
Longia, G.S., Agarwal, A.K., Thomas, R.J., Jain, P.N., and Saxena, S.K. 1982. Metrical study of rhomboid fossa of clavicle. *Anthropologischer Anzeiger* 40, 111–115.
Lordkipanidze, D., Jashashvili, T., Vekua, A., de León, M.S.P., Zollikofer, C.P.E., Rightmire, P.G., Pontzer, H., Ferring, R., Oms, O., Tappen, M., Bukhsianidze, M., Agusti, J., Kahlke, R., Kiladze, G., Martinez-Navarro, B., Mouskhelishvili, A., Nioradze, M., and Rook, L. 2007. Postcranial evidence from early *Homo* from Dmanisi, Georgia. *Nature* 449, 305–310.
Lorenzo, C., Arsuaga, J.L., and Carretero, J.M. 1999. Hand and foot remains from the Gran Dolina Early Pleistocene site (Sierra de Atapuerca, Spain). *Journal of Human Evolution* 37, 501–522.
Marchi, D., Walker, C.S., Wei, P., Holliday, T.W., Churchill, S.E., Berger, L.R., and deSilva, J.M. 2016. Thigh and leg remains of *Homo naledi*. *American Journal of Physical Anthropology* 159, 218–219.
Marchi, D., Walker, C.S., Wei, P., Holliday, T.W., Churchill, S.E., Berger, L.R., and DeSilva, J.M. 2017. The thigh and leg of *Homo naledi*. *Journal of Human Evolution* 104, 174–204.
Martin, R. 1928. *Lehrbuch der Anthropologie in systematischer Darstellung mit besonderer Berücksichtigung der anthropologischen Methoden*. Second edition. GustavFischer, Jena.
Martin, R. and Saller, K. 1957. *Lehrbuch der Anthropologie*. GustavFischer Verlag, Stuttgart.
Marzke, M.W. 1997. Precision grips, hand morphology, and tools. *American Journal of Physical Anthropology* 102, 91–110.
Mays, S., Steele, J., and Ford, M. 1999. Directional asymmetry in the human clavicle. *International Journal of Osteoarchaeology* 9, 18–28.
McHenry, H.M., Corruccini, R.S., and Howell, F.C. 1976. Analysis of an early hominid ulna from the Omo basin, Ethiopia. *American Journal of Physical Anthropology* 44, 295–304.
Melillo, S.M. 2016. The shoulder girdle of KSD-VP-1/1. In *The Postcranial Anatomy of* Australopithecus afarensis: *New Insights from KSD-VP-1/1*, Haile-Selassie, Y. and Su, D.F. (eds.). Springer, Netherlands, pp. 113–141.
Napier, J.R. 1965. Comment on "New discoveries in Tanganyika: their bearing on hominid evolution" by P.V. Tobias. *Current Anthropology* 5, 402–403.
Negri, J.H., Malavolta, E.A., Assunção, J.H., Gracitelli, M.E.C., Pereira, C.A.M., Bolliger Neto, R., Croci, A.T., and Ferreira Neto, A.A. 2014. Assessment of the function and resistance of sternoclavicular ligaments: a biomechanical study in cadavers. *Orthopaedics & Traumatology: Surgery & Research* 100, 727–731.
Nguyen, N.H., Pahr, D.H., Gross, T., Skinner, M.M., and Kivell, T.L. 2014. Micro-finite element (FE) modeling of the siamang (*Symphalangus syndactylus*) third proximal phalanx: the functional role of curvature and the flexor sheath ridge. *Journal of Human Evolution* 67, 60–75.
Niewoehner, W.A. 2000. *The Functional Anatomy of Late Pleistocene and Recent Human Carpometacarpal and Metacarpo-phalangeal Articulations*. Ph.D. Dissertation. University of New Mexico, Albuquerque.
Niewoehner, W.A. 2001. Behavioral inferences from the Skhul/Qafzeh early modern human hand remains. *Proceedings of the National Academy of Sciences USA* 98, 2979–2984.
Niewoehner, W.A., Weaver, A.H., and Trinkaus, E. 1997. Neandertal capitate-metacarpal articular morphology. *American Journal of Physical Anthropology* 103, 219–233.

Olivier, G. 1951. Technique de mesure des courbures de la clavicule. *Comptes Rendus de l'Association des Anatomistes* 69, 753–764.

Olivier, G. 1954. Corrélations des caractères de la clavicule. *Comptes Rendus de l'Association des Anatomistes* 1953, 248–254.

Oxnard, C.E. 1969. A note on the Olduvai clavicular fragment. *American Journal of Physical Anthropology* 29, 429–432.

Paraskevas, G., Natsis, K., Spanidou, S., Tzaveas, A., Kitsoulis, P., Raikos, A., Papaziogas, B., and Anastasopoulos, N. 2009. Excavated type of rhomboid fossa of the clavicle: a radiological study. *Folia Morphologica* 63, 163–166.

Partridge, T.C., Granger, D.E., Caffee, M.W., and Clarke, R.J. 2003. Lower Pliocene hominid remains from Sterkfontein. *Science* 300, 607–612.

Rice, W.R. 1989. Analyzing tables of statistical tests. *Evolution* 43, 223–225.

Richmond, B.G. 1998. *Ontogeny and Biomechanics of Phalangeal Form in Primates*. Stony Brook University, New York.

Richmond, B.G. 2007. Biomechanics of phalangeal curvature. *Journal of Human Evolution* 53, 678–690.

Rightmire, G.P. and Deacon, H.J. 1991. Comparative studies of Late Pleistocene human remains from Klasies River Mouth, South Africa. *Journal of Human Evolution* 20, 131–156.

Roach, N.T. and Richmond, B.G. 2015. Humeral torsion does not dictate shoulder position, but does influence throwing speed. *Journal of Human Evolution* 85, 206–211.

Schmid, P. 1983. Eine Rekonstruktion des Skelettes von A.L. 288-1 (Hadar) und deren Konsequenzen. *Folia Primatologica* 40, 283–306.

Schroeder, L., Scott, J.E., Garvin, H.M., Laird, M.F., Dembo, M., Radovčić, D., Berger, L.R., de Ruiter, D.J., and Ackermann, R.R. 2017. Skull diversity in the *Homo* lineage and the relative position of *Homo naledi*. *Journal of Human Evolution* 101, 1–12.

Schultz, A.H. 1930. The skeleton of the trunk and limbs of higher primates. *Human Biology* 2, 303–438.

Senut, B. 1981. *L'humérus et ses articulations chez les hominidés plio-pléistocènes*. Cahiers de Paléontologie (Paléoanthropologie). Éditions du Centre Nacional de la Recherche Scientifique, Paris.

Sokal, R.R. and Rohlf, F.J. 1995. *Biometry*, 3rd edition. Freeman and Co., New York.

Solan, M. and Day, M.H. 1992. The Baringo (Kapthurin) ulna. *Journal of Human Evolution* 22, 307–313.

Spencer, E.E., Kuhn, J.E., Huston, L.J., Carpenter, J.E., and Hughes, R.E. 2002. Ligamentous restraints to anterior and posterior translation of the sternoclavicular joint. *Journal of Shoulder and Elbow Surgery* 11, 43–47.

Stern, J.T. and Susman, R.L. 1983. The locomotor anatomy of *Australopithecus afarensis*. *American Journal of Physical Anthropology* 60, 279–317.

Susman, R.L. 1998. Hand function and tool behavior in early hominids. *Journal of Human Evolution* 35, 23–46.

Sutikna, T., Tocheri, M.W., Morwood, M.J., Saptomo, E.W., Jatmiko, Awe, R.D., Wasisto, S., Westaway, K.E., Aubert, M., Li, B., Zhao, J.-x., Storey, M., Alloway, B.V., Morley, M.W., Meijer, H.J.M., van den Bergh, G.D., Grün, R., Dosseto, A., Brumm, A., Jungers, W.L., and Roberts, R.G. 2016. Revised stratigraphy and chronology for *Homo floresiensis* at Liang Bua in Indonesia. *Nature* 532, 366–369.

Toussaint, M., Macho, G.A., Tobias, P.V., Partridge, T.C., and Hughes, A.R. 2003. The third partial skeleton of a Pliocene hominin (Stw 431) from Sterkfontein, South Africa. *South African Journal of Science* 99, 215–223.

Trinkaus, E. 1977. A functional interpretation of the axillary border of the Neanderthal scapula. *Journal of Human Evolution* 6, 231–234.

Trinkaus, E. 1983. *The Shanidar Neandertals*. Academic Press, New York.

Trinkaus, E. and Churchill, S.E. 1988. Neandertal radial tuberosity orientation. *American Journal of Physical Anthropology* 75, 15–21.

Trinkaus, E. and Villemeur, I. 1991. Mechanical advantages of the Neanderthal thumb in flexion: a test of an hypothesis. *American Journal of Physical Anthropology* 84, 249–260.

Tubbs, R.S., Shah, N.A., Sullivan, B.P., Marchase, N.D., Comert, A., Acar, H.I., Tekdemir, I., Loukas, M., and Shoja, M.M. 2009. The costoclavicular ligament revisited: a functional and anatomical study. *Romanian Journal of Morphology and Embryology* 50, 475–479.

Van den Bergh, G.D., Kaifu, Y., Kurniawan, I., Kono, R.T., Brumm, A., Setiyabudi, E., Aziz, F., and Morwood, M.J. 2016. *Homo floresiensis*-like fossils from the early Middle Pleistocene of Flores. *Nature* 534, 245–248.

Vandermeersch, B. and Trinkaus, E. 1995. The postcranial remains of the Régourdou 1 Neandertal: the shoulder and arm remains. *Journal of Human Evolution* 28, 439–476.

Voisin, J.-L. 2000. *L'épaule des hominidés. Aspects architecturaux et fonctionnels, références particulières à la clavicule*. Museum National d'Histoire Naturelle, Paris.

Voisin, J.-L. 2001. Évolution de la morphologie claviculaire au sein du genre *Homo*. Conséquences architecturales et fonctionnells sur la ceinture scapulaire. *L'Anthropologie* 105, 449–468.

Voisin, J.-L. 2004. Clavicule: approche architecturale de l'épaule et réflexions sur le statut systématique des néandertaliens. *Comptes Rendus Palevol* 3, 133–142.

Voisin, J.-L. 2006a. Clavicle, a neglected bone: morphology and relation to arm movements and shoulder architecture in primates. *Anatomical Record* 288, 944–953.

Voisin, J.-L. 2006b. Krapina and other Neanderthal clavicles: a peculiar morphology? *Periodicum Biologorum* 108, 331–339.

Voisin, J.-L. 2008. The Omo I hominin clavicle: archaic or modern? *Journal of Human Evolution* 55, 438–444.

Voisin, J.-L. 2010. L'architecture de l'épaule au sein du genre *Homo*: nouvelles interprétations. *L'Anthropologie* 114, 354–369.

Voisin, J.-L. 2012. Les caractères discrets des membres supérieurs: un essai de synthèse des données. *Bulletin et* Mémoires de la Societé d'Anthropologie de Paris 24, 107–130.

Voisin, J.-L. 2015. Australopithecine shoulders: new remains for old debate. In *Recent discoveries and Perspectives in Human Evolution*, Sankhyan, A.R. (ed.). British Archaeological Reports International Series S2719, Archaeopress, Oxford, England, pp. 11–21.

Voisin, J.-L. and Chevalier, T. in press. Les clavicules A63 et A91 de la Caune de l'Arago. In *Caune de l'Arago - Tautavel-en-Roussillon, Pyrénées-Orientales, France* –– Tome IX, De Lumley, H. (ed.). CNRS éditions, Paris.

Ward, C.V. 2007. Postcranial and locomotor adaptations of hominoids. In *Handbook of Paleoanthropology*, Tattersall, I., Henke, W., and Hardt, T. (eds.). Springer, New York, pp. 1011–1030.

Wiley, D.F. 2006. *Landmark Editor 3.0*. IDAV, University of California, Davis, California.

Williams, S.A., García-Martínez, D., Bastir, M., Meyer, M.R., Nalla, S., Hawks, J., Schmid, P., Churchill, S.E., and Berger, L.R. 2017. The vertebrae and ribs of *Homo naledi. Journal of Human Evolution* 104, 136–154.